Physics – Uspekhi **54** (6) 549 – 572 (2011)

REVIEWS OF TOPICAL PROBLEMS

PACS numbers: **12.60. – i**, 14.60.Pq, 25.30.Pt

Study of neutrino oscillations in long-baseline accelerator experiments

Yu G Kudenko

DOI: 10.3367/UFNe.0181.201106a.0569

Contents

Abstract. A review of the title subject is given. The phenomenology of neutrino oscillations in the framework of the so-called neutrino Standard Model (νSM) with three active neutrinos is considered. The recently completed long-baseline accelerator experiment K2K and currently in-progress MINOS and OPERA experiments are described in detail. The oscillation parameters obtained from the global analysis of all oscillation data are given. The short-baseline experiment MiniBooNE and its results on the search for light sterile neutrinos are discussed in detail. Considerable attention is given to searching for $\nu_\mu \to \nu_e$ oscillations and measuring the θ_{13} angle in muon neutrino experiments. The concept of the off-axis neutrino beam is reviewed. The T2K experiment, collecting statistics since early 2010, is described for its details and objectives. The NOνA experiment under construction and the next-generation beta beam and neutrino factory experiments are also discussed.

1. Introduction

Long-term experiments with solar and atmospheric neutrinos have led to the discovery of neutrino oscillations and have radically changed our understanding of neutrino physics, because this effect is possible only in the case of a nonzero neutrino mass. In the Standard Model, neutrinos are massless particles that cannot change their flavor and travel at the speed of light, and therefore do not mix, because the lepton number conservation laws were empirically postulated for three lepton families. But as follows from the oscillations, neutrinos have a small nonzero mass, they mix, and neutrino flavors (lepton numbers) are not conserved. This fundamental result was a direct experimental evidence pointing to the existence of new physics beyond the Standard Model and simultaneously initiated the study of this physics.

The history of neutrino oscillations traces back to Pontecorvo [1, 2], who proposed the hypothesis of $\nu \to \bar{\nu}$ oscillations via the mixing of two Majorana neutrinos by analogy with $K^0 \to \bar{K}^0$ oscillations. Because only the electron neutrino was known in the 1950s, Pontecorvo introduced the notion of a sterile neutrino, which is a neutral fermion and does not participate in weak interactions [3]. In 1968, Gribov and Pontecorvo suggested that neutrinos produced with a particular flavor can change their flavor (violate the lepton number) with the probability depending on the distance from the source [4]. Their work practically laid the groundwork for the experimental search for neutrino oscillations and proposed a high-sensitivity method of measuring small neutrino masses.

The first evidence of the existence of neutrino oscillations was obtained in the chlorine experiment by Davis et al. [5], in which they observed a deficit of the solar ν_es: the neutrino flux was measured at about 1/3 of that predicted by the Standard Solar Model [6].

Measurements of boron neutrinos by the Kamiokande [7–9] and Super-Kamiokande [10] Cherenkov detectors, which unambiguously identified solar neutrinos and separated them from the background due to measurement of the

Yu G Kudenko Institute for Nuclear Research
Russian Academy of Sciences,
prosp. 60-letiya Oktyabrya 7A, 117312 Moscow, Russian Federation
Tel. (7-496) 751 01 84
E-mail: kudenko@inr.ru

Received 26 Jule 2010, revised 11 November 2010
Uspekhi Fizicheskikh Nauk **181** (6) 569 – 594 (2011)
DOI: 10.3367/UFNr.0181.201106a.0569
Translated by E N Ragozin; edited by A M Semikhatov

direction of detected neutrinos and of the spatial correlation with the solar position, also showed that the neutrino flux was about 46% of the predicted one. Two radiochemical gallium experiments — the Soviet–American Gallium Experiment (SAGE) [11] and the GALLium EXperiment (GALLEX) [12], which detected solar neutrinos with the low energy threshold 0.23 MeV — also confirmed this effect.

Although these four independent experiments, radiochemical detectors, and Super-Kamiokande reliably measured the deficit of solar neutrinos, they did not provide an unambiguous answer to the question about the causes this effect. A model-independent proof of ν_e transitions into ν_μ and ν_τ was obtained in the Sudbury Neutrino Observatory (SNO) experiment [13], which used a heavy-water detector. Solar neutrinos were detected through both a charged current sensitive only to electron neutrinos and a neutral current sensitive to the total active neutrino flux from the Sun. Elastic neutrino scattering on the electron, which proceeds via both charged and neutral currents, was also measured and used as a check. It was discovered in this experiment that the electron neutrino flux is about 1/3 of the flux of all neutrino types measured through the neutral current. It was thereby proved that electron neutrinos, which are the only type emerging in the solar cycle, are converted to other neutrino types (ν_μ and ν_τ) on the way from the Sun to Earth.

An independent confirmation of neutrino oscillations with parameters characteristic of solar neutrinos was obtained in the long-baseline reactor experiment Kamioka Liquid scintillator Anti-Neutrino Detector (KamLAND) [14], which revealed a deficit of reactor antineutrinos, measured the spectrum distortion, and obtained the most accurate value for the squared-mass difference.

An unequivocal experimental discovery of the oscillations of atmospheric neutrinos was made at the Super-Kamiokande underground facility [15]. Due to the Cherenkov detector capability of measuring the direction and energy of the electrons and muons produced by atmospheric muon and electron neutrinos in the detector mass, it was determined that the experimentally measured muon neutrino flux was substantially lower than the calculated flux. The greatest discrepancy was observed for events in which neutrinos traveled through Earth in the upward direction. At the same time, the measured electron neutrino flux was in perfect agreement with the flux calculated under the assumption that the oscillations are absent. More recently, this result was confirmed by two long-baseline accelerator experiments: KEK-to-Kamioka (K2K) [16] and Main Injector Neutrino Oscillation Search (MINOS) [17], which discovered a deficit of the total number of muon neutrinos in the far detector in comparison with the neutrino flux expected in the absence of oscillations. Also discovered and measured in both experiments was a distortion of the muon neutrino spectrum shape in the far detector, which exhibited a sinusoidal dependence on L/E_ν (L is the muon flight path and E_ν is the neutrino energy), characteristic of oscillations, which was also observed in Super-Kamiokande [18]. The parameters of muon neutrino oscillations obtained in these three experiments are in excellent agreement with each other. This effect is well described by 'pure' oscillations of muon neutrinos to tau neutrinos with the squared mass difference $\sim 2 \times 10^{-3}$ eV^2 and a nearly maximal mixing, although alternative models are not excluded completely. For instance, the probability that decays of the muon neutrino into lighter particles might imitate neutrino oscillations was estimated at only 0.1% [18]. The question of mixed transitions, i.e., oscillations plus an admixture of other processes, remains open and is considered in Section 3.2, devoted to the MINOS experiment.

Oscillation experiments have revealed the existence of a nonzero neutrino mass and the mixing of neutrino flavors, but these experiments cannot yield the absolute mass scale, knowing which is fundamentally significant and is a window to new physics. Information about the neutrino mass can be derived from cosmological data and direct precision beta-decay measurements. Cosmological data are sensitive to the sum of masses of all neutrino mass states [19, 20], while tritium beta-decay measurements are most sensitive to the mass of the electron antineutrino [21].

Information about the nature of the neutrino is not provided by oscillation experiments, either. As is well known, all charged fermions (leptons and quarks) are Dirac particles. Unlike them, the neutrino has a zero charge, and neutrinos may therefore be Majorana fermions, i.e., be self-antiparticles. An unequivocal proof would be the experimental observation of neutrinoless double beta decay (see Refs [22–24]) resulting in violation of the total lepton number, which is possible only for Majorana neutrinos.

Currently, the study of neutrino oscillations is early in the long-term stage of precision measurements. One of the central parts in this long-term program is assigned to long-baseline accelerator experiments. The first two generations of such experiments are considered in detail in Section 3.6. These are the pioneering long-baseline K2K experiment completed in 2005, the MINOS and the Oscillation Project with Emulsion-tRacking Apparatus (OPERA) [25, 26] experiments, which are currently accumulating statistics, and the Tokai-to-Kamioka (T2K) [27] and NuMI (Neutrinos at the Main Injector) Off-Axis ν_e Appearance (NOνA) [28] second-generation experiments, which are intended to use an off-axis quasimonoenergetic muon neutrino beam optimized for measurements in the first oscillation maximum of atmospheric neutrinos. These experiments represent mainstream investigations involving accelerator neutrinos for the next 10–15 years and largely determine future trends in the accelerator neutrino physics.

In Section 4, the MiniBooNE (BooNE is the abbreviation of 'Booster Neutrino Experiment) short-baseline accelerator experiment [29] is also considered, whose main objective is to measure the muon neutrino oscillations in the $\Delta m^2 \sim 1$ eV^2 region, i.e., to verify the result obtained in the Liquid Scintillator Neutrino Detector (LSND) experiment [30].

The investigation of neutrino properties in neutrino factories or with beta beams, which is planned for the distant future, is also considered briefly. We note that many aspects of the physics of neutrino oscillations and the principles of accelerator oscillation experiments are discussed at some length in Refs [31–35].

2. Phenomenology of neutrino oscillations

Neutrino oscillations are described by the so-called neutrino Standard Model (νSM), which is the minimal model comprising the mixing of three neutrino types. The physics of neutrino oscillations is described by a unitary matrix U [36] that relates three types of active neutrinos with left-handed helicity, ν_e, ν_μ, and ν_τ, to the mass eigenstates ν_1, ν_2, and ν_3 with the

respective masses m_1, m_2, and m_3:

$$\begin{pmatrix} \nu_e \\ \nu_\mu \\ \nu_\tau \end{pmatrix} = \begin{pmatrix} U_{e1} & U_{e2} & U_{e3} \\ U_{\mu 1} & U_{\mu 2} & U_{\mu 3} \\ U_{\tau 1} & U_{\tau 2} & U_{\tau 3} \end{pmatrix} \begin{pmatrix} \nu_1 \\ \nu_2 \\ \nu_3 \end{pmatrix}. \quad (1)$$

The unitarity of U signifies that for each mass state ν_1, ν_2, ν_3, the total probability of an admixture of ν_e, ν_μ, or ν_τ is equal to unity. In the general case, the elements of this matrix should be complex quantities. The matrix U can be parameterized by three mixing angles θ_{12}, θ_{23}, θ_{13} and three physical CP-odd phases. In a form convenient for physical analysis, the matrix U can be represented as the product of four matrices:

$$U = \begin{pmatrix} 1 & 0 & 0 \\ 0 & \cos\theta_{23} & \sin\theta_{23} \\ 0 & -\sin\theta_{23} & \cos\theta_{23} \end{pmatrix} \times \begin{pmatrix} \cos\theta_{13} & 0 & \sin\theta_{13}\exp(-i\delta) \\ 0 & 1 & 0 \\ -\sin\theta_{13}\exp(i\delta) & 0 & \cos\theta_{13} \end{pmatrix} \times \begin{pmatrix} \cos\theta_{12} & \sin\theta_{12} & 0 \\ -\sin\theta_{12} & \cos\theta_{12} & 0 \\ 0 & 0 & 1 \end{pmatrix} \begin{pmatrix} \exp\frac{i\alpha_1}{2} & 0 & 0 \\ 0 & \exp\frac{i\alpha_2}{2} & 0 \\ 0 & 0 & 1 \end{pmatrix}. \quad (2)$$

The elements of matrix (2) and the mixing angles are related as

$$\frac{|U_{e2}|^2}{|U_{e1}|^2} = \tan^2\theta_{12}\,, \quad \frac{|U_{\mu 3}|^2}{|U_{\tau 3}|^2} = \tan^2\theta_{23}\,,$$

$$U_{e3} = \sin\theta_{13}\exp(-i\delta)\,. \quad (3)$$

It is shown below that the probability of neutrino oscillation depends on the three mixing angles, two squared mass differences $\Delta m^2_{12} = m_2^2 - m_1^2$ and $\Delta m^2_{23} = m_3^2 - m_2^2$, and the CP-odd Dirac phase δ. The Majorana phases α_1 and α_2 exert no effect on neutrino flavor oscillations because they result in a violation of the total lepton number, which is conserved in the course of the oscillations. The first of the four matrices in (2) is associated with atmospheric neutrino oscillations, and the parameters Δm^2_{23} and θ_{23} are the 'atmospheric parameters.' The second matrix describes the so-called reactor neutrino oscillations, because the upper bound on the θ_{13} angle was set by the Chooz reactor experiment [37], which measured $\bar\nu_e \to \bar\nu_e$ transitions. The value of the CP-odd phase δ is unknown. The physics of solar neutrino oscillations is described by the third matrix, and Δm^2_{12} and θ_{12} are the 'solar oscillation parameters.' The physics of the fourth matrix, which is related to the Majorana neutrino mass, manifests itself in double beta decay. The physical ranges for the mixing angles and the phase δ are defined as

$$0 \leqslant \theta_{12}\,,\ \theta_{23}\,,\ \theta_{13} \leqslant \frac{\pi}{2}\,, \quad 0 \leqslant \delta \leqslant 2\pi\,. \quad (4)$$

The condition

$$\Delta m^2_{12} + \Delta m^2_{23} = \Delta m^2_{13} \quad (5)$$

is also satisfied. We emphasize that the analysis of solar neutrino experiments (see Refs [38, 39]) allows concluding that $\Delta m^2_{12} > 0$, i.e., $m_2 > m_1$, while the sign of Δm^2_{23} is unknown. The so-called normal neutrino mass hierarchy corresponds to the case $\Delta m^2_{23} > 0$, and the inverse mass hierarchy is that with $\Delta m^2_{23} < 0$. The question of which mass order is realized in reality is fundamentally significant for the understanding of the nature of neutrino mass and the mechanism of mixing [40, 41].

The general expression for the probability of vacuum oscillations between two types of neutrinos, α and β, is

$$P(\nu_\alpha \to \nu_\beta) = \underbrace{\delta_{\alpha\beta} - 4\sum_{k>j} \mathrm{Re}[U^*_{\alpha j}U_{\beta j}U_{\alpha k}U^*_{\beta k}]\sin^2\frac{\Delta m^2_{jk}L}{4E_\nu}}_{CP=1} + \underbrace{2\sum_{k>j}\mathrm{Im}[U^*_{\alpha j}U_{\beta j}U_{\alpha k}U^*_{\beta k}]\,7mm(6)}$$

where α, $\beta = e, \mu, \tau$, E_ν is the neutrino energy and L is the path length, i.e., the distance from the neutrino source to the detector in which the neutrino is detected. The CP-even terms in this expression are indicated with $CP = 1$ and the CP-odd term with $CP \neq 1$. The corresponding expression for the antineutrino is obtained by changing $U \leftrightarrow U^*$, which results in the change of sign of the second, CP-odd, term.

Several physical inferences can be drawn from (6).

1. If neutrinos are massless particles, i.e., $\Delta m^2_{ij} = 0$, then $P(\nu_\alpha \to \nu_\beta) = \delta_{\alpha\beta}$. Therefore, neutrino flavor violation is definitely possible only for a nonzero neutrino mass.

2. Expression (6), which describes oscillations in the vacuum, neglects the effects of the neutrino interaction with matter as the neutrino propagates from a source to a detector, which we discuss in Section 6. Because neutrinos are detected via weak interaction, no flavor change occurs at the instant of neutrino detection.

3. Transitions of neutrino flavors may be measured by two methods. An 'appearance' experiment searches for ν_β neutrinos in a beam that initially consisted of only ν_α neutrinos. A 'disappearance' experiment measures a deficit in the known initial ν_α flux in comparison with the value predicted in the absence of oscillations. We emphasize that in the latter case, the distortion of the initial shape of the neutrino spectrum should be observed.

4. It follows from expression (6) that CP violation may show up only in the 'appearance' experiment, because $\mathrm{Im}(U^*_{\alpha j}U_{\beta j}U_{\alpha k}U^*_{\beta k}) = 0$ for $\alpha = \beta$.

5. Neutrino oscillations do not decrease the total neutrino flux: they merely redistribute it between different flavors. As indicated above, the unitarity of the matrix U implies that

$$\sum_\beta P(\nu_\alpha \to \nu_\beta) = 1\,. \quad (7)$$

However, the following remark is in order: if the three known neutrino generations (active neutrinos) may undergo conversion to sterile neutrinos, which are not detected via weak interactions in a detector, then despite the detection of all types of active neutrinos, a decrease in the total flux of active neutrinos is to be observed in the experiment.

Specific expressions for the oscillation of muon neutrinos in the vacuum, derived from general expression (6), are as follows:

$$P(\nu_\mu \to \nu_\mu) = 1 - 4\sum_{k>j} |U_{\mu j}|^2 |U_{\mu k}|^2 \sin^2 \frac{\Delta m_{jk}^2 L}{4E_\nu}$$
$$= 1 - \sin^2 2\theta_{23} \sin^2 \frac{\Delta m_{13}^2 L}{4E_\nu} + \left(\frac{1}{2} \cos^2 \theta_{12} \sin^2 2\theta_{23} \right.$$
$$\left. - \sin\theta_{13} \sin^2 \theta_{23} \sin 2\theta_{23} \sin 2\theta_{12} \cos\delta \right)$$
$$\times \sin \frac{\Delta m_{12}^2 L}{4E_\nu} \sin \frac{\Delta m_{13}^2 L}{4E_\nu} + O\left(\frac{\Delta m_{12}^2}{\Delta m_{13}^2}\right) + O(\sin^2 \theta_{13}) , \quad (8)$$

$$P(\nu_\mu \to \nu_e) = \sin^2 \theta_{23} \sin^2 2\theta_{13} \sin^2 \frac{\Delta m_{13}^2 L}{4E_\nu}$$
$$+ \frac{1}{2} \sin 2\theta_{23} \sin 2\theta_{12} \cos^2 \theta_{13} \sin\theta_{13} \sin \frac{\Delta m_{12}^2 L}{2E_\nu}$$
$$\times \sin \frac{\Delta m_{13}^2 L}{2E_\nu} \cos\delta - \sin 2\theta_{23} \sin 2\theta_{12} \cos^2 \theta_{13} \sin\theta_{13}$$
$$\times \sin \frac{\Delta m_{12}^2 L}{2E_\nu} \sin^2 \frac{\Delta m_{13}^2 L}{4E_\nu} \sin\delta + O\left(\frac{\Delta m_{12}^2}{\Delta m_{13}^2} \sin^2 \theta_{13}\right). \quad (9)$$

Because $|\Delta m_{12}^2| \ll |\Delta m_{13}^2| \approx |\Delta m_{23}^2|$ and the typical baselines of accelerator experiments for investigating oscillations in the 'atmospheric' parameter region amount to several hundred kilometers, the contribution of the terms containing Δm_{12}^2 in expressions (8) and (9) is small, and expressions (8) and (9) can be represented as [42, 43]

$$P(\nu_\mu \to \nu_\mu) \simeq 1 - \sin^2 2\theta_{23} \cos^4 \theta_{13} \sin^2 \frac{\Delta m_{13}^2 L}{4E_\nu}$$
$$- P(\nu_\mu \to \nu_e) , \quad (10)$$

$$P(\nu_\mu \to \nu_e) \simeq \sin^2 2\theta_{13} \sin^2 \theta_{23} \sin^2 \frac{\Delta m_{13}^2 L}{4E_\nu} . \quad (11)$$

If the neutrino energy and the experiment baseline are selected such that the oscillation probability $P(\nu_\mu \to \nu_e)$ is maximum, i.e., $(\Delta m_{13}^2 L)/(4E_\nu) = \pi/2 + n\pi$, then

$$P(\nu_\mu \to \nu_e) \approx \frac{1}{2} \sin^2 2\theta_{13} . \quad (12)$$

We consider a simplified version with two neutrino types. This approach is frequently used in the analysis of experimental data. In this case, there is one mixing angle θ and CP violation does not occur. If we take ν_e and ν_μ, for example, then the two-flavor neutrino mixing can be written, by analogy with the mixing of quarks, as

$$\begin{pmatrix} \nu_e \\ \nu_\mu \end{pmatrix} = \begin{pmatrix} \cos\theta & \sin\theta \\ -\sin\theta & \cos\theta \end{pmatrix} \begin{pmatrix} \nu_1 \\ \nu_2 \end{pmatrix} . \quad (13)$$

The electron neutrino, which is produced in the W-boson–electron interaction, is a linear superposition of two mass eigenstates, ν_1 and ν_2. Observing the effect of neutrino mixing requires experiments in which processes depending on the mass eigenstates are measured. If neutrino flavors (types) are manifestations of the weak interaction, then the mass states can manifest themselves in the course of propagation of neutrinos as free particles through the vacuum. For ν_e produced with a momentum $\mathbf{p}$ at the point $x = 0$ at the instant $t = 0$, the wave function can be written as a superposition of the wave functions of two plane waves corresponding to the mass eigenstates ν_1 and ν_2,

$$\left|\nu_e(t=0)\right\rangle = \cos\theta |\nu_1\rangle + \sin\theta |\nu_2\rangle . \quad (14)$$

In the propagation through the vacuum, at $t > 0$, we have

$$\left|\nu(\mathbf{x}, t)\right\rangle = \exp\left[\mathrm{i}(\mathbf{px} - E_1 t)\right] \cos\theta |\nu_1\rangle$$
$$+ \exp\left[\mathrm{i}(\mathbf{px} - E_2 t)\right] \sin\theta |\nu_2\rangle , \quad (15)$$

where

$$E_i = \sqrt{p^2 + m_i^2} = p\sqrt{1 + \frac{m_i^2}{p^2}} \approx p + \frac{m_i^2}{2p} , \quad (16)$$

if $m_i \ll p$. At $t > 0$, the neutrino wave function therefore has the form

$$|\nu(t)\rangle = \cos\theta |\nu_1\rangle + \exp(\mathrm{i}\phi) \sin\theta |\nu_2\rangle \quad (17)$$

with the phase

$$\phi = \frac{m_1^2 - m_2^2}{2p} t . \quad (18)$$

A neutrino that was a purely electron one at $t = 0$ is no longer such at $t > 0$; owing to the existence of the phase ϕ, it acquires an admixture of a muon neutrino. The probability that a neutrino produced as ν_e interacts with a detector as ν_μ, i.e., the electron-to-muon neutrino transition probability, is given by

$$P(\nu_e \to \nu_\mu) = \left|\langle \nu_\mu | \nu(t)\rangle\right|^2 = \sin^2 2\theta \sin^2 \frac{\pi x}{L} , \quad (19)$$

with the oscillation length

$$L = \frac{4\pi p}{\Delta m^2} = \frac{4\pi E_\nu}{\Delta m^2} \quad (20)$$

and $\Delta m^2 = m_2^2 - m_1^2$. Accordingly,

$$P(\nu_e \to \nu_e) = 1 - \sin^2 2\theta \sin^2 \frac{\pi x}{L} . \quad (21)$$

The probabilities of these transitions oscillate over a length L. The amplitude of these oscillations, which is defined by the mixing angle θ, reaches a maximum at $\theta = 45^\circ$.

3. First-generation long-baseline experiments

3.1 K2K experiment

The K2K experiment (Japan) [44] was the first long-baseline accelerator experiment for studying muon neutrino oscillations in the region of 'atmospheric' parameters. In this experiment, the oscillations of muon neutrinos were to show up in the form of two effects. The first effect was the deficit of the total number of neutrinos detected in Super-Kamiokande in comparison with the flux expected from the near detector. The second effect was the distortion of the energy spectrum of neutrinos detected in Super-Kamiokande characteristic of oscillations with Δm_{23}^2 and $\sin^2 2\theta_{23}$ in comparison with the neutrino spectrum expected in the absence of oscillations. Because the dominant oscillation mode for muon neutrinos with the energy ~ 1 GeV is the conversion of muon neutrinos into τ neutrinos, the simplified version with two neutrino

flavors considered in Section 2 can be used for data analysis. In the framework of this approach, the probability that ν_μ with an energy E_ν is converted into ν_τ on traveling a distance L in the vacuum is given by

$$P(\nu_\mu \to \nu_\tau) = \sin^2 2\theta \sin^2\left(\frac{1.27\Delta m^2[\mathrm{eV}^2]\, L[\mathrm{km}]}{E_\nu[\mathrm{GeV}]}\right), \quad (22)$$

where θ is the mixing angle between the mass and active states and Δm^2 is the squared mass difference of the mass states.

The neutrino beam obtained from the KEK 12 GeV proton synchrotron was measured by two detectors: the near neutrino detector located at the distance 300 m from the target in which pions were produced and the Super-Kamiokande (SK) Cherenkov detector [45] with the total mass 50 kt, which was 250 km away. The near neutrino detector consisted of a water Cherenkov detector 1 kt in mass and a system of segmented scintillation detectors.

3.1.1 Neutrino beam. The secondary particles (pions, kaons) in the energy range from 0 to ≈ 10 GeV were produced by 12 GeV protons hitting an aluminum target. Positively charged particles, primarily π^+s, with momenta 2–3 GeV/c were focused in the forward direction by a system of two pulsed horn magnets, which produced a toroidal magnetic field, and then decayed into a muon and a muon neutrino, $\pi^+ \to \mu^+\nu_\mu$, in a decay volume 200 m in length. Focusing the pion beams by two horns afforded an approximately 20-fold increase in the flux of neutrinos with the energy >0.5 GeV in the Super-Kimiokande direction.

To reduce the absorption and uncontrollable pion production in the air, the decay volume was filled with helium at the pressure 1 atm. The beam dump located at the end of the decay volume consisted of 3.5 m thick iron, 2 m thick concrete, and a region of soil about 60 m long. The beam dump absorbed all particles except neutrinos and high-energy muons. Located immediately after the concrete absorber was a muon detector (an ionization chamber and a set of silicon detectors), which detected the high-energy part of the muon spectrum with the momentum above 5.5 GeV/c and measured the profile of the neutrino beam.

Due to the high intensity of the muon flux ($\sim 10^4\ \mu^+$ per cm^2 per s), the direction of the neutrino beam was monitored and controlled within 3 mrad for each accelerator pulse, which enabled monitoring the spectrum and the neutrino flux at the far detector with the accuracy about 1%.

Throughout the experiment, the neutrino beam was pointed in the direction of SK within ± 1 mrad, which ensured the neutrino flux and spectrum stability at SK within 1%. The spectra of all neutrino types flying in the direction toward SK, i.e., at a zero angle to the proton beam direction, which were obtained by Monte Carlo simulations, are plotted in Fig. 1. The contamination of muon neutrinos in the beam was 97.3% in the near detector and 97.9% in SK. The admixtures of other neutrino types in the near detector and SK (given in parentheses) were $\nu_e/\nu_\mu \sim 0.013(0.009)$, $\bar\nu_\mu/\nu_\mu \sim 0.015(0.012)$, and $\bar\nu_e/\nu_\mu \sim 1.8 \times 10^{-4}(2.2 \times 10^{-4})$.

3.1.2 Near neutrino detector. The near neutrino detector (Fig. 2), whose primary purpose was to measure and monitor the direction and intensity of the neutrino beam as well as the energy spectrum of neutrinos prior to oscillations, consisted of two main systems: a water Cherenkov detector and a segmented scintillation detector, which comprised a Scintillating Fiber Detector (SciFi) with a water target, an electromagnetic calorimeter of lead glass (LG) (it was replaced with an active segmented scintillation detector (SciBar) at the second stage of the experiment), and a high-energy muon detector — Muon Range Detector (MRD).

One-kiloton Cherenkov detector. The Cherenkov detector was a miniature version of the Super-Kamiokande detector: it had water as the neutrino target and the same photomultipliers (PMTs) for detecting Cherenkov light. A cylindrical tank 10.8 m in diameter and 10.8 m in height was filled with pure water. The total detector (water target) mass was 1000 t. This volume was divided into the inner detector (a cylinder 8.6 m in diameter and 8.6 m in height viewed by 680 PMTs, each 50 cm in diameter) and the outer one (with 68 PMTs), which was the veto system for charged particles entering the detector. The inner-detector PMTs were spaced at 70 cm, which allowed covering about 40% of the surface

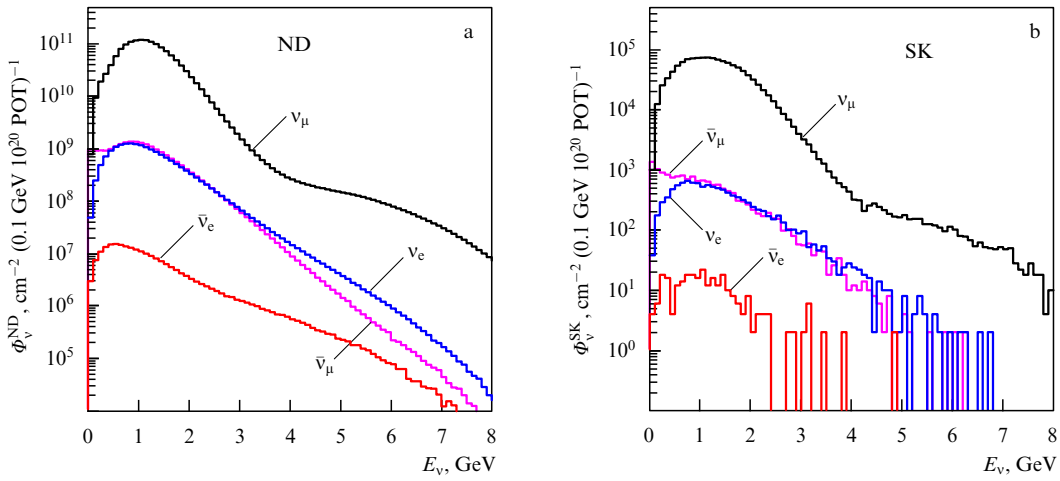

Figure 1. Neutrino energy spectra in (a) the near detector (ND) and (b) in the Super-Kamiokande (SK) detector obtained on the basis of MC simulations of the K2K neutrino beam. The contamination of muon neutrinos is equal to 97.3% in the near detector and 97.9% in the SK detector. The admixtures of other neutrino types in the near and SK (in parentheses) detectors are $\nu_e/\nu_\mu \sim 0.013(0.009)$, $\bar\nu_\mu/\nu_\mu \sim 0.015(0.012)$, and $\bar\nu_e/\nu_\mu \sim 1.8 \times 10^{-4}(2.2 \times 10^{-4})$.

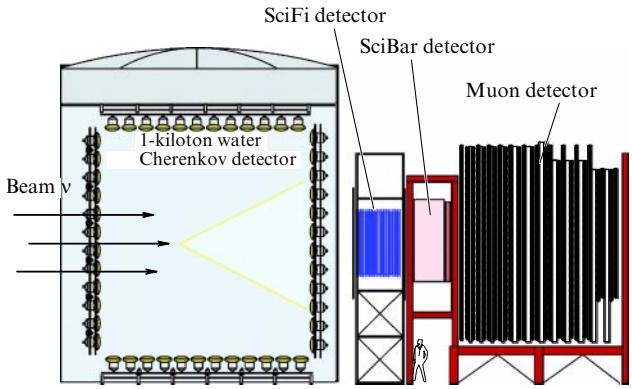

Figure 2. Schematic view of the near K2K detector during the second stage of experiment. At the first stage of the experiment, a lead glass calorimeter was used instead of the SciBar segmented scintillation detector.

area by their photocathodes. The sensitive volume of the detector, in which neutrinos were detected, was a cylinder 4 m in diameter and 2 m in length along the neutrino beam, with the mass 25 t. The physical parameters of a neutrino event in this detector — the coordinates of the neutrino interaction point, the number of Cherenkov rings, the particle type, and the momentum — were determined according to the same algorithm that was used in the analysis of events in SK. It is noteworthy that this tank had been previously used in the calibration experiment performed jointly by the Kamiokande and Irvine–Michigan–Brookhaven detector (IMB) collaboration teams at KEK for the experimental verification of the criteria used to identify charged particles in water Cherenkov detectors [46].

The spatial coordinates of the neutrino interaction point in the detector were determined from PMT timing information. Only single-neutrino events during an accelerator pulse were analyzed because a water Cherenkov detector does not allow reconstructing neutrino interaction vertices in the case of several events per pulse. With the known vertex position, the number of Cherenkov rings and their directions were determined by a maximum-likelihood procedure. Each ring is then classified as μ-like or e-like. The e-like rings corresponded to particles that did not produce electromagnetic showers ($\mu^{\pm}, \pi^{\pm}$) and the e-like rings corresponded to $e^{\pm}$ and photons. The momentum of each particle was determined from the intensity of Cherenkov light in the ring. Events with less than 200 photoelectrons were classified as events with the energy completely absorbed in the inner detector. The spatial resolution was about 15 cm for single-ring events and about 40 cm for multiple-ring events, and the angular resolution was about 1°. The muon momentum resolution was 2.0–2.5% throughout the neutrino energy range. A high quality of particle identification was reached: only 0.3% of the muons resulting from neutrino interactions were identified as electrons and 3.3% of electron neutrino events were identified as muon-like events.

SciFi detector. The Scintillating Fiber Detector with the cross section 2.6×2.6 m^2 consisted of alternating layers of scintillating fibers (20 layers) with the total weight 6 t and of water (19 layers) with the weight about 5.5 t [47, 48]. The main function of this detector, which had capabilities complementary to those of the 1-kiloton detector, consisted in measurements of the high-energy part of the neutrino spectrum and of quasielastic and inelastic reactions at neutrino energies inaccessible to the water detector.

SciBar detector. The full-active highly segmented scintillation detector [49, 50] with the total weight 15 t and dimensions $3 \times 3 \times 1.7$ m^3 consisted of 15000 scintillating strips, each 3 m in length, 2.5 cm in width, and 1.3 cm in thickness. An electromagnetic spaghetti-type calorimeter located behind the segmented detector permitted identifying reactions with the participation of electron neutrinos and measuring the ν_e admixture in the muon neutrino beam, as well as studying the production of π^0 in neutrino interactions. A special feature of this detector was the high efficiency of the detection of charged low-energy particles produced in neutrino interactions. For instance, the proton detection threshold was about 450 MeV/c and the efficiency of reconstructing events with a short isolated track $\geqslant 10$ cm long was as high as $\approx 99\%$.

MRD. The main function of the MRD was to monitor the neutrino beam stability (direction, profile, and energy) and to measure the spectrum of muons that were produced in the SciFi and SciBar detectors and reached the MRD, which enabled measuring the high-energy part of the neutrino spectrum. The MRD had a cross section of 7.6×7.6 m^2 and consisted of 12 steel plates (four plates 10 cm thick in the front part of the detector and eight succeeding plates 20 cm thick) located between 13 layers of vertical and horizontal drift tubes. The total thickness of the iron layers, which was equal to 2.0 m, was sufficient for measuring the muon energy in the range between 0.3 GeV and 2.8 GeV with the energy resolution about 0.12 GeV and the spatial resolution of muon tracks about 5°.

3.1.3 Super-Kamiokande far detector. The Super-Kamiokande facility [45], which is a water Cherenkov detector with the volume 50000 m^3, is located in Japan, under Ikenoyama mountain. Because the thickness of the rock is about 1 km, which corresponds to 2700 m of the water equivalent, cosmic muons with energies below 1.3 TeV do not reach the detector, and the high-energy muon flux decreases by about a factor of 10^6 and is 5×10^{-8} cm^{-2} s^{-1} sr^{-1}.

The detector, a giant tank 39 m in diameter and 42 m in height filled with pure water, is divided into two detectors: an inner one and an outer one. The entire volume of the inner detector with the height 36.2 m and radius 6.9 m and weight 32 kt is viewed by 11146 spherical Hamamatsu R3600 photomultipliers. The PMTs are arranged in a 70 cm pitch array on the walls, top, and bottom of the detector. The photocathode of each PMT is 50 cm in diameter; the total photocathode area, i.e., the active part of the photomultipliers, covers 40% of the entire detector surface.

The optically isolated water volume with the weight 18 kt (the outer detector), surrounding the inner detector, is viewed by 1885 PMTs 20 cm in diameter. In this detector, the water layer thickness is equal to 2.60–2.75 m. The detector operates as an active 4π-veto-detector for charged particles and also serves as a passive shield from the neutrons and photons from the mountain rock. The water transparency in the detector is about 100 m for Cherenkov radiation at the wavelength 420 nm.

The Super-Kamiokande detector detects neutrinos in the energy range from 4.5 MeV to 1 TeV. Each PMT of the inner detector has a dynamic range from 1 to 300 photoelectrons. For low-energy events (primarily for the study of solar neutrinos), the energy of a charged particle is determined

from the number of PMT hits, while high-energy events are measured from the total number of photoelectrons of all PMTs. The dimension, shape, and direction of the Cherenkov cone are used for event identification: a single-ring μ-like, single-ring e-like, or multiple-ring event. The momentum resolution of the detector was equal to 2.4% for muons with the momentum 1 GeV/c.

The time synchronization between the pulse of the proton synchrotron at KEK and Super-Kamiokande was provided via the Global Positioning System (GPS) with the precision of 50 ns [51]. This precision allowed observing the beam microstructure in the neutrino events detected by the SK and enabled suppressing the atmospheric neutrino background to a negligible level.

3.1.4 Data analysis and results. If oscillations of muon neutrinos exist, then, as noted above, this effect should manifest itself in the following form: (i) deficit of the muon neutrino events in Super-Kamiokande in comparison with the number of such events expected in the absence of the oscillations; (ii) distortion of the shape of the energy spectrum of detected neutrinos in comparison with the spectrum expected in the absence of oscillations.

The near detector measured the initial flux and neutrino spectrum near the decay volume (prior to possible oscillations). These measurements were then extrapolated to the far detector using the ratio between the neutrino fluxes at the far (F) and near (N) detectors,

$$R(\mathrm{F/N}) = \frac{\Phi^{\mathrm{SK}}(E_\nu)}{\Phi^{\mathrm{ND}}(E_\nu)}\,, \tag{23}$$

obtained by Monte Carlo simulations (assuming the absence of oscillations), where $\Phi^{\mathrm{SK}}(E_\nu)$ is the neutrino spectrum in the Super-Kamiokande expected in the absence of oscillations and $\Phi^{\mathrm{ND}}(E_\nu)$ is the neutrino spectrum measured in the near detector. If the neutrinos were produced by a point-like source, the quantity $R(\mathrm{F/N}) \sim 1/L^2$, where L is the source–detector distance, would be independent of the neutrino energy.

The decay volume for the Super-Kamiokande looks like a point-like source, but this condition is not satisfied for the near detector, because pion decays occur over a length of 200 m. Owing to the finite dimensions of the decay volume and the near detector, the ratio R depends on the neutrino energy, the details of target geometry and decay volume, and the cross sections for production of pions and their focusing by the magnetic field, as well as on the cross sections for the neutrino interaction with detector materials and the geometry of the detectors and their parameters.

The results of the Hadron Production Experiment (HARP) [53], which performed high-precision measurements of the cross sections of positive pion production in the interaction of 12.9 GeV/c protons with a thin aluminum target, were used in modeling $R(\mathrm{F/N})$.

The systematic uncertainties in $R(\mathrm{F/N})$ included uncertainties arising from the multiple interaction of pions in the target and those related to the beam profile and the uncertainty in the magnetic field. Furthermore, to increase the reliability of the data, the $R(\mathrm{F/N})$ ratio was calculated by two other independent methods: using the Cho-CERN model [53] and using the data of the pion monitor that measured the spectrum of pions with momenta >2 GeV/c, which corresponded to the 1 GeV energy threshold for neutrinos. In all three approaches, the absolute $R(\mathrm{F/N})$ values and the energy dependence of this parameter agreed nicely with each other, as shown in Ref. [54].

Measurements were performed from 1999 to 2004. During this period, the integral proton flux accumulated at the target was equal to 1.05×10^{20} (0.92×10^{20} was used for the oscillation analysis). In the SK detector, the total number of PMTs were used during the first phase of the experiment (K2K-I), while during the second part of the beam time (K2K-II), the density of PMTs was approximately two times lower. The following criteria were applied to select the accelerator neutrino events: a 1.0 μs time slot synchronized with a proton accelerator pulse; the absence of any signals for 30 μs before the event; a minimal number of electrons in the signal amplitude, equal to 200 (K2K-I) and 94 (K2K-II); and the absence of any signal in the outer detector for those events whose energy was completely absorbed by the inner detector. Furthermore, the minimal energy liberated in the detector had to be to 30 MeV and the reconstructed vertex of the event had to be inside the 22.5 kt inner volume.

In total, 112 events satisfying the selection criteria indicated above were detected. Fifty-eight of them were classified as single-ring muon-like events. In these events, the energy of the muons was completely deposited in the inner SK detector.

The expected number $N(\mathrm{SK})$ of neutrino events in the SK detector (in the absence of oscillations) was determined from the measured number $N(\mathrm{kt})$ of neutrino events in the 1-kiloton detector as

$$N(\mathrm{SK}) = N(\mathrm{kt})\, R(\mathrm{F/N})\, \frac{\mathrm{POT_{SK}}}{\mathrm{POT_{kt}}}\, \epsilon_{\mathrm{SK}}\,, \tag{24}$$

where $R(\mathrm{F/N})$ is the ratio between neutrino fluxes at the far and near detectors (expression (23)), $\mathrm{POT_{SK,kt}}$ is the integral proton flux at the target (proton on target) used in the data analysis in the SK and 1-kiloton detector, and ϵ_{SK} is the efficiency of neutrino event selection in the SK detector. All known systematic errors and their correlations were included in the analysis.

Based on the neutrino flux measurements in the near detector (1 kt), the total number of events expected in the SK during the whole period of data taking was equal to $158.1^{+9.2}_{-8.6}$. The main sources of systematic uncertainties in the evaluation of the number of events were the uncertainties in the active volume of the 1-kiloton detector and the SK detector ($^{+4.9\%}_{-4.8\%}$) and the uncertainties in $R(\mathrm{F/N})$ ($^{+2.9\%}_{-2.9\%}$) [54]. The expected spectrum shape of single-ring muon-like events (assuming the absence of oscillations) and the spectrum uncertainties were calculated in the same way as the number of events.

The oscillation analysis for neutrinos of two flavors, which was performed by the maximum-likelihood method, involved a comparison of the quantities measured in the far detector and the expected quantities obtained by extrapolating the near detector data under the no-oscillation assumption. As discussed above, the effect of muon neutrino oscillations, if any, was to show up as a deficit of neutrino events and distortion of the energy spectrum of the neutrinos observed in the SK detector. Therefore, the likelihood function was defined as the product of the function $\mathcal{L}_{\mathrm{norm}}$, which depends on the number of events detected by SK, and the function $\mathcal{L}_{\mathrm{shape}}$, which depends on the spectrum shape of the neutrino events. Furthermore, systematic errors, which were treated as adjustable parameters, were taken into

account by an additional likelihood function $\mathcal{L}_{\rm syst}$. The total likelihood function was defined as

$$\mathcal{L} = \mathcal{L}_{\rm norm}\ \mathcal{L}_{\rm shape}\ \mathcal{L}_{\rm syst}\,. \tag{25}$$

In $\mathcal{L}_{\rm norm}$, 112 events were used, and 58 single-ring events were analyzed in $\mathcal{L}_{\rm shape}$. The systematic uncertainties of the analysis included systematic errors in determining the neutrino spectrum in the near detector, the error in $R(\mathrm{F/N})$, and the uncertainties in the cross sections for neutrino–nuclei interactions, in determining the efficiency and energy scale of the SK detector, and in the overall normalization. The main error in the analysis of the measured shape of the neutrino spectrum was determined by the accuracy of the calibration of the SK energy scale.

To extract the oscillation parameters, the flux and spectrum shape $\Phi^{\rm SK}(E_\nu)$ of SK neutrinos were calculated using the spectrum $\Phi^{\rm ND}(E_\nu)$ measured in the near detector and $R(\mathrm{F/N})$ as

$$\Phi^{\rm SK}(E_\nu) = \Phi^{\rm ND}(E_\nu)\, R(\mathrm{F/N})\,(1 - P(E_\nu, \Delta m^2, \sin^2 2\theta))\,, \tag{26}$$

where $P(E_\nu, \Delta m^2, \sin^2 2\theta)$ is the muon neutrino oscillation probability [see expression (22)]. The parameters Δm^2 and $\sin^2 2\theta$ were varied for determining the highest value of $\mathcal{L}$. As a result, the values $\Delta m^2 = 2.8 \times 10^{-3}$ eV^2 and $\sin^2 2\theta = 1.0$ were obtained from the best fit of the number of events as well as of the spectrum shape [54]. For these values, the number of neutrino events in the SK detector, which were determined using expression (26), was equal to 107.2, which was in excellent agreement with the number of experimental events. Figure 3 shows the measured neutrino spectrum (single-ring muon-like events). The dashed curve in Fig. 3 corresponds to the absence of oscillations and the solid curve corresponds to the best fit to the experimental spectrum using the oscillation parameters given above. The probability of experimental data description with these parameters, which was tested by the Kolmogorov–Smirnov method, was 37%, while the no-oscillation description of the data corresponded to the probability 0.07%. A combined analysis of the number of events and the spectrum shape ruled out the absence of oscillations at the level of 4.3σ or, in other words, the probability that this effect was due to a statistical fluctuation was equal to 0.0015% [54]. Therefore, the first long-baseline neutrino experiment K2K brilliantly confirmed the effect of atmospheric neutrino oscillations discovered by Super-Kamiokande and opened up a new era of precision neutrino oscillation measurements in long-baseline accelerator experiments.

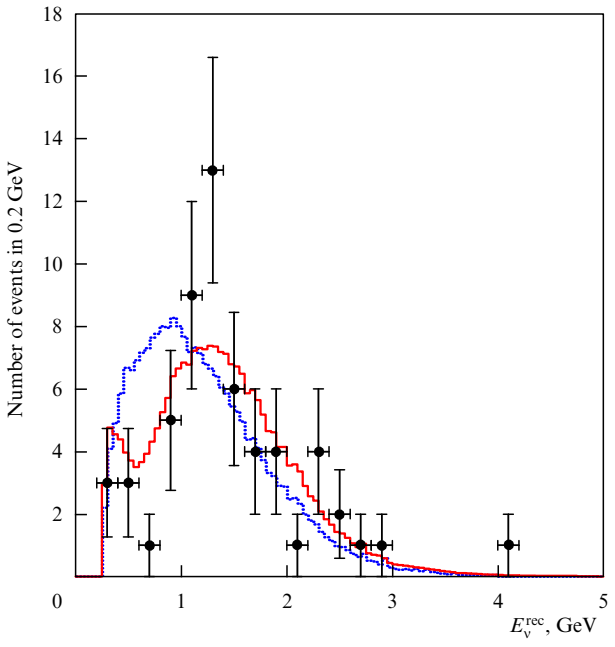

Figure 3. Neutrino spectrum measured by the SK detector. Shown are the single-ring muon-like events in which the muon energy was completely absorbed in the sensitive volume of the detector. Fifty-eight such events were observed in total. The dotted line shows the spectrum expected in the absence of oscillations and the solid line represents the best fit to the experimental spectrum in the presence of muon neutrino oscillations with the parameter values $\Delta m^2 = 2.8 \times 10^{-3}$ eV^2 and $\sin^2 2\theta = 1.0$. Both curves are normalized to the number of the observed events.

3.2 MINOS experiment

The primary goal of the MINOS experiment (E Fermi National Accelerator Laboratory (Fermilab), USA) is to study muon neutrino oscillations and measure Δm^2_{23} with the precision better than 10% [17]. The experiment uses a muon neutrino beam in the energy range from one to several tens of GeV. These neutrinos arise from the decays of pions and kaons, which are produced in 120 GeV proton collisions with a graphite target, in a 675 m long decay channel 2 m in diameter, in which the air pressure is about 1 Torr. The hadrons produced in the target are focused by a system of two toroidal horn magnets. We note that the hadron momentum and the neutrino energy spectrum depend on the position of the magnets relative to the target.

The optimal sensitivity to oscillation parameters is obtained when the target is inserted into the first horn, which ensures the neutrino spectrum maximum at the energy ≈ 3 GeV in the direction of 0 degrees relative to the proton beam. In this configuration, the neutrino beam consists of muon neutrinos (92.9%) with an admixture of 5.5% $\bar\nu_\mu$ and 1.3% ($\nu_e + \bar\nu_e$). When the distance of the first horn from the target increases to 100 cm, the neutrino spectrum maximum shifts to the energy 6 GeV; when the distance is 250 cm, the broad neutrino spectrum has the maximum at 9 GeV.

After traveling the distance of 725 km through Earth, neutrinos are detected by a 5.4 kt far detector, which is located at the depth of 714 m in the Soudan Mine (Minnesota). A 1 kt near detector, located 1 km away from the target, measures the neutrino spectrum and the beam composition near the target; it has the same configuration as the far detector.

In this experiment, the characteristic ratio L/E_ν between the baseline and the average energy of the neutrino beam is ≈ 240 km per GeV, and therefore MINOS has the highest sensitivity to neutrino oscillations in the interval $\Delta m^2 \approx (2{-}3) \times 10^{-3}$ eV^2.

3.2.1 Far and near neutrino detectors. Both detectors are tracking sampling calorimeters with alternating layers of passive (steel) and active (scintillator) materials embedded in a strong magnetic field [55]. The identity of detector structures permits eliminating many systematic errors related to neutrino interactions in detectors and to detection of secondary particles.

The far MINOS detector, whose general view is shown in Fig. 4, comprises two supermodules separated by 1.1 m. The basic detector structure is a set of octagonal planes, each of which consists of a steel plate 2.54 cm thick and a plastic

scintillator 1 cm thick. The first supermodule consists of 248 planes and the second of 236 planes. The planes are spaced 2 cm apart in both detectors. Each scintillator plane consists of 192 optically isolated strips 4 cm wide up to 8 m in length. The strips are arranged at the angles $+90°$ and $-90°$ in the neighboring planes.

The scintillation light is collected with the aid of wavelength shifting (WLS) fibers embedded into the strips. The further transportation of the light from both ends of the WLS fibers to 16-anode PMTs is provided by clear optical fibers. Each supermodule is magnetized to the field strength 1.5 T due to a 15 kA current flowing through the coil shown in Fig. 4.

The detector detects muon neutrinos due to interactions via the charged current $\nu_\mu + \mathrm{Fe} \to \mu^- + X$ by identifying a muon track and a hadron shower in this process. The muon track curvature is used to determine the energy of the muons that escape from the detector and to separate the muon neutrino component from the $\bar{\nu}_\mu$ admixture, which is about 6%.

The energy of those muons whose track is entirely inside the detector is measured from their range. For muons traveling perpendicular to the detector planes, the momentum resolution $(\sigma_p/p)^2 = 0.06^2 + (0.045/p[\mathrm{GeV}])^2$ has been obtained. The energy of a hadron shower is determined by summing up the signals from individual strips that form a cluster identified as hadronic. The energy resolution of a hadron shower is $\sigma_E/E \approx 0.55/\sqrt{E[\mathrm{GeV}]}$. Muon neutrinos are also detected via the neutral current, $\nu_\mu + \mathrm{Fe} \to \nu_\mu + X$. Only a hadron shower without a muon track is present in this case. Electron neutrinos are detected via the charged current by detecting an electromagnetic shower, which is different in shape from the hadronic one. The total energy of a neutrino event is defined as the sum of energies of the highest-energy track and the attendant shower.

The near detector consists of 282 octagonal planes of the size 4×6 m^2. The strips in the near detector are substantially shorter in length than those in the far detector. In contrast to the far detector, only one end of each fiber in the near detector is read out; the other end is coated with a thin aluminum layer to ensure a mirror reflection of reemitted light. Owing to the shorter fiber length, the light yield of the scintillation detectors in this one-end configuration is comparable to the light yield of the far detector with two-end readout.

It is also noteworthy that the neutrino interaction rate per unit mass is approximately 10^6 higher in the near detector, which necessitated the use of faster electronics having a shorter 'dead' time.

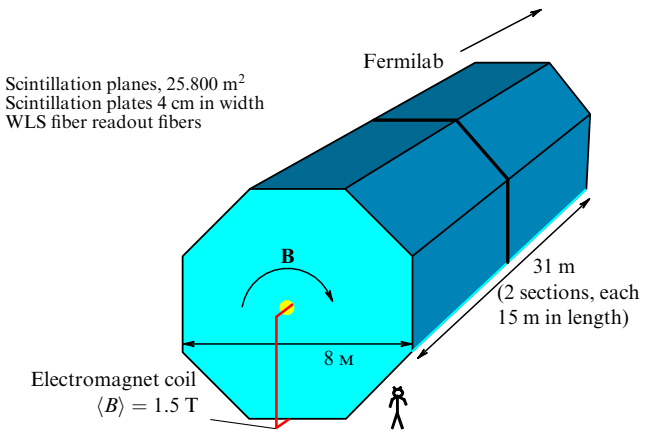

Figure 4. Schematic view of the far MINOS detector.

To measure the energies of muons, electrons, and hadrons and reconstruct the neutrino energy, the same algorithm is used as in the far detector. A unique feature of the near and far detectors is the presence of a magnetic field, which permits making a distinction between the ν_μ and $\bar{\nu}_\mu$ charged currents by the curvature of the μ^- and μ^+ tracks. This allows studying neutrino and antineutrino oscillations separately. After applying all kinematic parameters in the analysis of muon tracks, the efficiency of identifying muon neutrinos via a charged current was 74% in the far detector and 67% in the near one.

3.2.2 Results. The neutrino energy spectrum measured for charged current events in the near detector is extrapolated to the far detector by Monte Carlo simulations, which use the real beam geometry and detector parameters. To reduce uncertainties in the prediction of the neutrino spectrum in the far detector, the neutrino spectrum in the near detector was modeled for nine different beam configurations, and a comparison was made with the spectra collected for these configurations in the near detector [17, 56]. The main sources of systematic errors in the oscillation analysis are the normalization, which is known to within 4%, the accuracy of determining the hadron shower energy (10.3%), and the uncertainty in estimating the background from neutral currents, which satisfies the criteria for the selection of a hadron shower from charged currents and is identified as a charged current ($\approx 50\%$). The uncertainties due to the normalization and the hadron shower, which primarily affect the error in Δm^2, are respectively $\pm 0.081 \times 10^{-3}$ eV^2 and $\pm 0{,}052 \times 10^{-3}$ eV^2. The uncertainty due to neutral currents makes the main contribution to the systematic error in the mixing parameter $\sin^2 2\theta$ and is equal to ± 0.16.

Measurements with atmospheric neutrinos were performed in 2003 and the physics run with the neutrino beam from the accelerator began in 2006. The results obtained after two years of data taking are displayed in Fig. 5, which shows the ratio between the experimental data and the predictions made under the no-oscillation assumption, as a function of the neutrino energy. In total, 848 events were detected in the far detector, while the number of events expected in the absence of oscillations was 1065 ± 60 for the exposure of 3.36×10^{20} protons on target.

The values $\Delta m^2 = (2.43 \pm 0.13) \times 10^{-3}$ eV^2 and $\sin^2 2\theta > 0.90$ (90% CL) were obtained from the analysis [57]; the allowed region of Δm^2 and $\sin^2 2\theta$ is shown in Fig. 6. The figure also shows the Super-Kamiokande and K2K results, as well as the oscillation parameter region reported by the MINOS collaboration in the first publication. The results of these experiments are in remarkable agreement with each other. Of special note is the following fact: using different neutrino energies and detectors that were totally different from those in Super-Kamiokande and K2K, MINOS obtained an absolutely independent confirmation of the results of these experiments. A preliminary analysis of the data corresponding to 7.2×10^{20} protons on target yields the oscillation parameters with smaller errors: $\Delta m^2 = (2.35 + 0.11 - 0.08) \times 10^{-3}$ eV^2 and $\sin^2 2\theta > 0.91$ (90% CL) [60].

A direct search for $\nu_\mu \to \nu_e$ oscillations was simultaneously conducted in the experiment. In this case, the main source of background is due to the decays of neutral pions

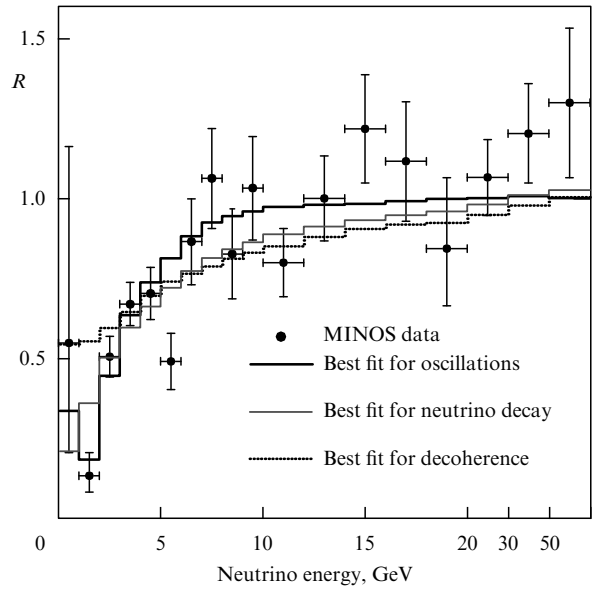

Figure 5. Energy dependence of the ratio R of the number of neutrino events detected in the far MINOS detector to the number predicted in the absense of oscillations [57]. The bold solid histogram shows the best fit obtained assuming the $\nu_\mu \to \nu_\tau$ oscillations and the mixing of two neutrino types; the solid and dotted histograms show the best fit for alternative models: the neutrino decay into lighter particles [58] and the quantum neutrino decoherence [59].

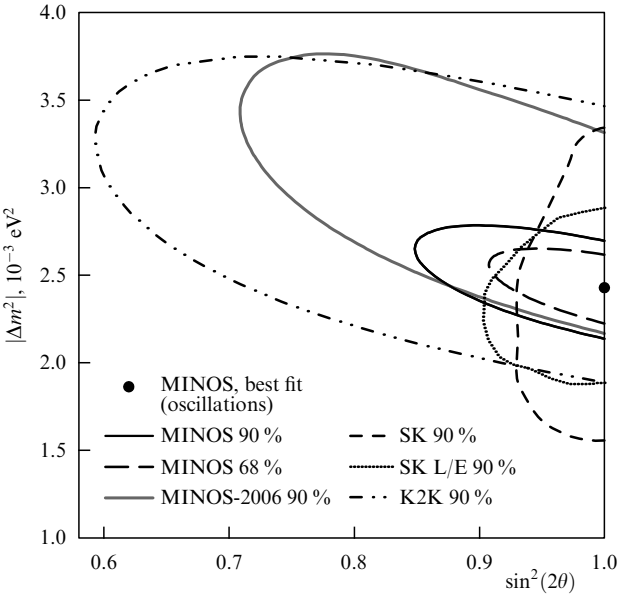

Figure 6. Regions for the Δm^2 and $\sin^2 2\theta$ oscillation parameters obtained in the MINOS experiment [57]. Also given are the data of the Super-Kamiokande, K2K, and the first MINOS result published in 2006. The L/E result was obtained in the measurement of the sinusoidal dependence of neutrino oscillations in the SK experiment [18].

produced in the detector in neutrino interactions via neutral currents. The analysis of the data collected in the far detector for the exposure of 7.0×10^{20} protons on target (POT), allowed selecting 54 candidates for ν_e with the expected background of $49.1 \pm 7.0(\text{stat.}) \pm 2.7(\text{syst.})$ events [61]. This result allowed obtaining a bound on the θ_{13} angle: $2\sin^2 2\theta_{13} \sin^2 \theta_{23} < 0.12(0.20)$ (90% CL) for normal (inverse) mass hierarchy and $\delta = 0$, which is a small improvement of the bound obtained by the Chooz reactor experiment.

The standard interpretation of the results of the Super-Kamiokande, K2K, MINOS, solar, and KamLAND reactor experiments is the mixing between the active neutrino types (flavors) participating in weak interactions. Precision measurements of the Z-boson decay width suggest that only three active neutrino families exist [62], but the existence of so-called sterile neutrinos ν_s, which do not participate in weak interactions, is not excluded. For instance, sterile neutrinos with a mass $\leqslant 1$ keV, whose existence does not contradict the oscillation data, may participate in the mechanism of neutrino mass formation [63] and play a significant role in solving several cosmological and astrophysical problems [64, 65].

Although Super-Kamiokande excluded the interpretation of the deficit of atmospheric muon neutrinos in the squared mass difference region $\Delta m^2 \sim 2 \times 10^{-3}$ eV^2 via pure $\nu_\mu \to \nu_s$ transitions in favor of the pure $\nu_\mu \to \nu_\tau$ conversion, broad possibilities remain for mixed transitions [66, 67]. If $\nu_\mu \to \nu_s$ transitions are possible, then, in addition to the deficit of muon neutrinos detected in the far MINOS detector via charged currents, a deficit should also be observed in the detection of muon neutrinos via neutral currents (exchange via Z^0) and the energy spectrum of such events in the far detector should be distorted.

The first measurement of this kind performed in the MINOS experiment did not find muon-to-sterile neutrino transitions [68]. But a quantitative analysis showed that muon neutrinos may transform into sterile ones with the probability about 50% (at the level of 90% CL) [69]. Therefore, the question of whether the deficit of muon neutrinos in the Super-Kamiokande, K2K, and MINOS experiments is attributable to pure $\nu_\mu \to \nu_\tau$ transitions or an addition exists in the form of the $\nu_\mu \to \nu_s$ transitions is still open. It is also noteworthy that the active-to-sterile neutrino decay (without oscillations, $\Delta m^2_{23} \to 0$) as an alternative to oscillations is excluded at a level of 5.4σ [70].

MINOS also presented the first results of oscillation measurements involving a muon antineutrino beam. We emphasize that conducting these measurements is a more difficult task because it is impossible to obtain a pure beam (muon antineutrinos account for only 40%, muon neutrinos amount to about 58%, and the admixture of $\nu_e + \bar{\nu}_e$ amounts to 2.0%) and because antineutrino interaction cross sections are smaller than the neutrino interaction cross sections. Preliminary data confirm the existence of antineutrino oscillations, but the antineutrino oscillation parameters differ from those characteristic of muon neutrino oscillations [60]. The accumulation of statistics with the antineutrino beam is underway and it is too early to make any fundamental inferences from these results.

3.3 OPERA experiment

The main goal of the long-baseline OPERA experiment is the search for the direct transition of muon neutrinos to τ neutrinos in the region of atmospheric oscillation parameters. This experiment uses the neutrino beam directed from CERN to the underground laboratory Gran Sasso, Italy (CNGS: CERN Neutrinos to Gran Sasso), which accommodates a neutrino detector located 730 km away from the neutrino source. Although the highest oscillation probability for this baseline corresponds to the neutrino

energy about 1.5 GeV, τ neutrinos can be detected only when their energies are sufficiently high. The main reaction enabling ν_τ detection is the quasielastic scattering $\nu_\tau + n \to \tau + p$, which may proceed when the neutrino energy exceeds the minimal energy, $E_{\nu_\tau} > m_\tau + m_\tau^2/2m_N \approx 3.5$ GeV. In view of the energy dependence of the cross section of charged current quasielastic neutrino scattering with a τ lepton production, it is reasonably safe to suggest that the neutrino beam energy required for the efficient production of τ leptons must be even higher. Interestingly, the ν_τ energy required for the reaction $\nu_\tau + e \to \nu_e + \tau$ must be $E_{\nu_\tau} > m_\tau^2/2m_e \approx 3$ TeV.

A 400 GeV proton beam is extracted from the Super Proton Synchrotron (SPS) accelerator and transported to a helium-cooled graphite target. The positive pions and kaons produced in the target are focused into a parallel beam by a system consisting of two magnetic lenses: a horn and a reflector. In the decay volume 1000 m long, the pions and kaons decay into muon neutrinos and muons to form a muon neutrino beam with a broad neutrino energy spectrum — from 5 GeV to 25 GeV (the average energy is 17 GeV) — at a zero angle to the proton beam direction [71]. The $\bar{\nu}_\mu$ admixture is about 4% and the admixture of ν_e and $\bar{\nu}_e$ is less than 1%. The contamination of ν_τ from D_s decays in the beam of muon neutrinos is negligible at these energies.

The experiment used only the far detector, whose general view is shown in Fig. 7. The neutrino target with the total mass about 1.35 kt comprises two supermodules, each consisting of plates made of a passive material (iron, lead) and thin active plates, which are nuclear photoemulsions. The heavy passive material (lead) is used as the target in which neutrinos experience interactions and the emulsion is used for reconstructing the tracks of charged particles resulting from neutrino interactions. The main detector element is a 'brick' $10.2 \times 12.7 \times 7.5$ cm^3 in size consisting of 56 lead plates 1 mm in thickness and 57 emulsion plates 45 μm thick each. The facility contains about 200,000 such bricks arranged into two supermodules. The ν_τ appearance signature is the detection of a decay of the τ lepton (with the lifetime $\tau_\tau \sim 10^{-13}$ s, $c\tau_\tau \sim 87$ μm) in the emulsion and the study of the topology of its subsequent decays with the emission of an electron, a muon, or hadrons. The identification of a τ lepton is provided by its decay products; the main decay modes are given below with approximate branching ratios:

$$\nu_\tau + N \to \begin{cases} \mu^- \bar{\nu}_\tau \nu_\mu - 17\%, \\ e^- \bar{\nu}_\tau \nu_e - 18\%, \\ h^- \bar{\nu}_\tau n(\pi^0) - 50\%. \end{cases} \qquad (27)$$

A specific feature of these decays, used in the experiment, is the so-called kink — a sharp change in the momentum direction (> 20 mrad) for the produced particles relative to the τ-lepton momentum, as illustrated in Fig. 8. A kink in a track for a path about 1 mm (Fig. 8a) permits identifying a τ-lepton decay into a charged particle and a neutrino. The main source of the background is the decays of charged particles resulting from the interaction of muon neutrinos via charged currents in the detector and having a decay topology close that of τ leptons (Fig. 8b). To identify this process, the occurrence of the 'wrong' sign of a muon emerging from the kink and the presence of a muon emerging from the muon neutrino interaction point in the lead plate are used. The 'brick' that has a high probability to contain the neutrino interaction vertex is determined from charged

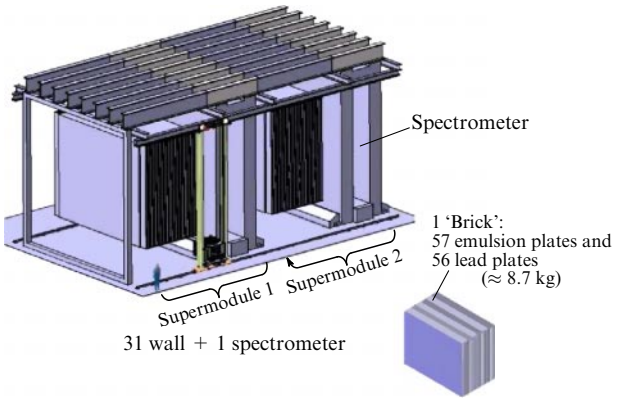

Figure 7. Schematic view of the OPERA detector.

particle tracks, which are measured by muon spectrometers located behind the supermodules. The spectrometers consist of active elements (12 planes of 8 m long drift tubes) and dipole magnets, which induce the field about 1.5 T. The muon spectrometers measure the muon momentum and charge.

This system allows obtaining a high efficiency in the determination of muon charge (the probability of incorrect identification is 0.1–0.3%), the spatial resolution better than 1 μm for charged particle tracks, and the momentum resolution $\Delta p/p \leqslant 0.20$ in the momentum region below 25 GeV/c. A large veto system located in front of the first module identifies neutrino interactions in the mountain rock around the hall or in the material in front of the detector. The 'bricks' that saw neutrino events are then extracted from their supermodule for developing plates and studying the in-emulsion tracks.

For the integral luminosity 4.5×10^{19} POT per year, about 10 ν_τ are expected to be detected via charged currents for the squared mass difference $\Delta m^2 \simeq 2.4 \times 10^{-3}$ eV^2 for five years of data taking. In this case, the background is assumed to be about one event. It is noteworthy that the number of ν_τ expected due to oscillations depends quadratically on Δm^2 because $\Delta m^2 \ll L/E_\nu$ [see expressions (19)

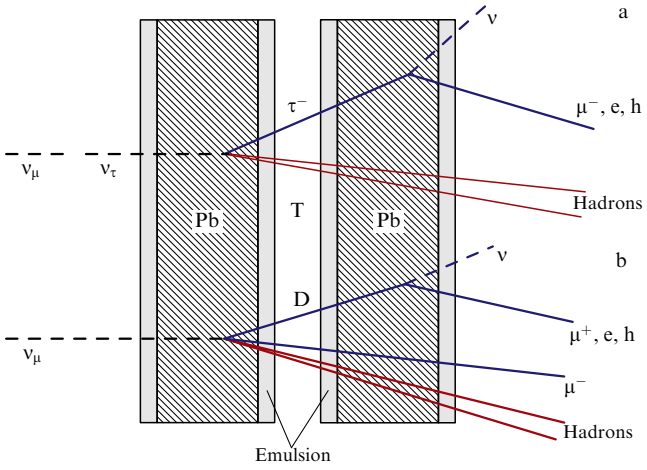

Figure 8. Topology of the main events involving a 'kink': (a) τ lepton decays into a charged particle and a neutrino; (b) main background process involving the production and decay of charmed mesons (D). T is a transparent cellulose base 200 μm in thickness coated on either side with two emulsion layers 45 μm thick each. The lead plates are 1 mm thick.

and (20)]. That is why 16 events are expected for $\Delta m^2 = 3.0 \times 10^{-3}$ eV^2 and 6 events are expected for $\Delta m^2 = 2.0 \times 10^{-3}$ eV^2 at the same background level.

After a short CNGS beam channel commissioning run without the detector neutrino target in 2006, the experiment was started and data taking began for a low proton beam intensity and partly installed 'bricks' (about 40% of the total number) in September 2007. Three hundred nineteen neutrino events were detected during the physics run [72], in agreement with the expectation of 300 events. The integral intensity 1.8×10^{19} POT was achieved in the 2008 run, and about 1700 neutrino interactions were detected in the neutrino target material. Online identification and extraction of the 'bricks' in which neutrino interactions occurred and the procedure of the analysis of the first neutrino events are described in detail in Refs [73, 74]. The efficiency of locating the 'brick' in which a neutrino event occurred was 88.3%; the efficiency of reconstructing the event vertex in the selected 'brick' was about 90% for charged currents and about 80% for neutral ones [75].

In the 2009 experiment, the integral intensity about 3.5×10^{19} POT was accumulated, and the total 2008–2009 integral luminosity was about 4.2×10^{19} protons on target, which enabled collecting about 4000 neutrino events in the detector target. The detection of one to two $\nu_\mu \to \nu_\tau$ events is expected from the analysis of these data. An important stage of the data analysis is the measurement and reconstruction of charmed particle production events. The first such events with a muon track have been successfully identified, and their analysis will enable significantly improving the understanding of the physical background and testing the reconstruction algorithm for events involving τ leptons [76].

Upon analyzing about 35% of the data accumulated in the experiment, the first candidate event for ν_τ was discovered [77]. A magnified image of this event with particles near the point of neutrino interaction with a distinct kink in the track is shown in Fig. 9. The decay topology corresponds to the chain $\tau^- \to \nu_\tau + \rho^- \to \nu_\tau + \pi^- + \pi^0$. This event is in good agreement with the expected number 0.54 ± 0.13 of τ neutrinos, the background for these events being estimated at the level of 0.018 ± 0.007 events. The statistical significance of this event as a ν_τ interaction in the detector is about 2.4σ.

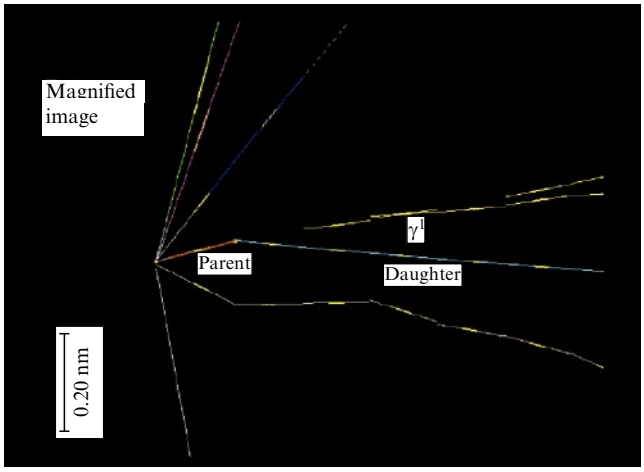

Figure 9. First neutrino event with a τ lepton decay found in the OPERA experiment [78].

4. MiniBooNE short-baseline experiment

The main task of the MiniBooNE experiment, which is conducted, like MINOS, at Fermilab, is to search for the $\nu_\mu \to \nu_e$ and $\bar{\nu}_\mu \to \bar{\nu}_e$ processes in the region $\Delta m^2 \leqslant 1$ eV^2 and to prove or disprove the effect of neutrino oscillations discovered in the LSND experiment in Los Alamos [30], which does not agree with the standard scheme of three weakly interacting neutrino types with two independent nonzero Δm^2 values. An explanation of this effect in the case of its independent verification would call for an extension of the νSM and the introduction of one or several light sterile neutrinos. Different models incorporating sterile neutrinos were considered in Refs [40, 79].

The MiniBooNE detector [80] is 541 m away from the target in which pions are produced by protons with the momentum about 9 GeV/c. The beryllium target is located inside a magnetic focusing system, which permits increasing the neutrino flux intensity at the point of detector location by about a factor of six, as well as collecting statistics with positive and negative pions, i.e., studying both neutrino and antineutrino oscillations. The pions produced in proton–nucleus collisions decay in flight through the 50 m long decay channel to produce a neutrino beam with the energy up to 3 GeV and the highest intensity at about 700 MeV. The π^+ decays produce a pure beam of muon neutrinos with a small (about 0.5%) contamination of electron neutrinos. In the operation with negative pions, the beam consists primarily of muon antineutrinos with a rather large (about 16%) admixture of muon neutrinos and a small (less than 1%) admixture of electron neutrinos and antineutrinos. The antineutrino energy spectrum lies in the 0–3 GeV range with the intensity maximum at 400 MeV.

The detector is a 6.1 m sphere filled with pure mineral oil (CH_2) weighing 818 tons and viewed by 1280 PMTs located in the inner sphere with the radius 5.75 m. The photomultipliers cover 10% of the sphere surface. The fiducial volume weighs 445 t. In the outer detector volume, 240 PMTs were used to detect signals from incoming external particles and the outgoing particles from the inner volume. The MiniBooNE detector is a combination of Cherenkov and scintillation detectors, wherein the charged particles produced due to neutrino interaction in the fiducial volume are identified by the instantaneous Cherenkov signal (the rings due to charged particles, as in the SK detector) and a delayed scintillation signal. An event is identified as a neutrino event if it coincides in time with an accelerator beam pulse and the number of PMT hits in the outer volume is less than six and the number of PMT hits in the inner detector is more than 200. These constraints allow substantially suppressing the background due to cosmic particles (decreasing it by about a factor of 1000).

In the search for the $\nu_\mu \to \nu_e$ process, the main reaction used to detect electron neutrinos is the quasielastic scattering via a charged current

$$\nu_e + {}^{12}\mathrm{C} \to e^- + X. \tag{28}$$

Measurement of the ring of Cherenkov light from the electrons allows determining the electron energy and direction. As in SK, electrons are identified by the characteristic shape of the ring (a diffuse spot due to an electromagnetic shower). It is noteworthy that the detector does not distinguish between photons and electrons because the

Cherenkov rings have the same shape in both cases. The energy detector resolution is about 11% for $E_\nu \leqslant 1$ GeV. The main background processes are neutral pion production via neutral currents (asymmetric $\pi^0 \to \gamma\gamma$ decays imitate the false signal from ν_e when the low-energy photon is not recovered) and the admixture of electron neutrinos in a muon neutrino beam. It is planned to record about 1000 $\nu_\mu \to \nu_e$ oscillations if the LSND result is correct and to confirm or disprove the results of this experiment at a statistically significant level.

4.1 Results

After three years of accumulating statistics, the first results of the search for the $\nu_\mu \to \nu_e$ transition were reported in early 2007 [29]. Figure 10 shows the reconstructed energy spectrum of electron neutrinos (to be more precise, candidates for electron neutrinos). No excess of neutrinos above the background ($22 \pm 19 \pm 35$ events) expected for the oscillation parameters discovered by the LSND was found in the $475 < E_\nu^{QE} < 1250$ MeV energy range used in the oscillation analysis. The dotted histogram in Fig. 10 shows the spectrum with the excess of electron neutrinos corresponding to the best fit in the oscillation analysis added to the background.

Thus, when a model with two types of neutrinos was used to predict muon-to-electron neutrino conversion under the assumption that $CP = 1$ and $CPT = 1$, the LSND result was excluded at 98% CL. But an excess of events above the background ($96 \pm 19 \pm 20$) was observed in the experiment in the energy region below 475 MeV. This excess above the background, which cannot be explained as a consequence of oscillations, calls for further investigations. A subsequent data analysis in the low-energy region 200–300 MeV also revealed an excess of electron events [81], which resulted in the total excess of 129 ± 43 events in the 200–470 MeV energy range [82].

The first results of MiniBooNE measurements with a muon antineutrino beam, which were based on the integral value 3.39×10^{20} POT, agree, to within statistical errors, with the expected background throughout the measured energy range from 200 to 3000 MeV [83]. No excess of events was observed in the high-energy region (> 475 MeV), where the oscillation analysis was performed. No excess of events was observed for the antineutrino energies 200–475 MeV, either (61 event for the expected background of 61.5 ± 11.7 events), unlike the excess of events recorded in the measurements with the neutrino beam. The next result with the antineutrino beam was published after the analysis of the data corresponding to 5.66×10^{20} POT [84]. An excess of events characteristic of $\bar\nu_\mu \to \bar\nu_e$ oscillations with $\Delta m^2 = 0.1-1.0$ eV^2 was discovered, which, according to the MiniBooNE collaboration, is consistent with the LSND result [84]. But this statement appears to be too categorical in view of the fact that the excess of events is about 2.8σ for the antineutrino energies above 475 MeV.

The MiniBooNE results can be summarized as follows: (a) no oscillations were discovered for neutrinos with energies above 475 MeV; (b) an explanation for the excess of ν_e events for energies below 475 MeV has not been found; (c) an excess of $\bar\nu_e$ events at energies exceeding 475 eV has been discovered, which is consistent with the LSND data.

Therefore, it is possible to draw a preliminary conclusion that MiniBooNE has failed to solve the LSND problem and the further accumulation of statistics appears to be ineffective. Most likely, it would be necessary to stage a radically different experiment to arrive at the final solution to this problem.

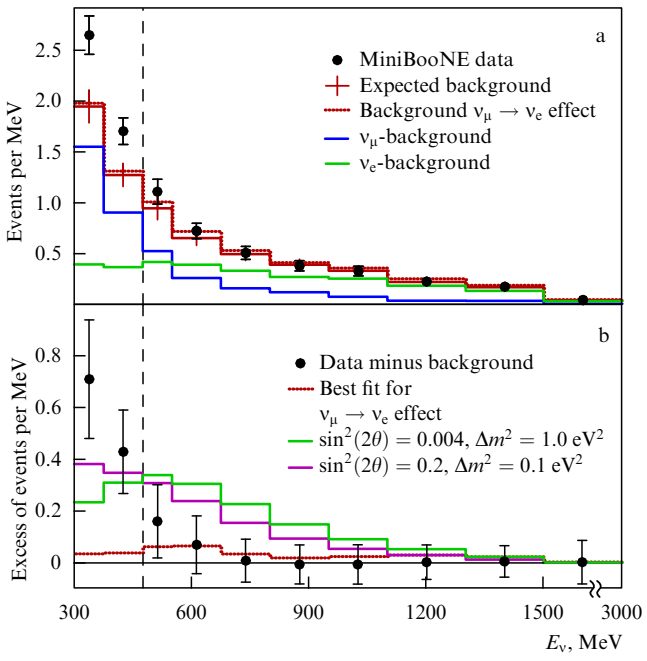

Figure 10. Electron neutrino spectrum obtained in the MiniBooNE experiment [29]. (a) Energy spectrum of electron neutrinos. The points show experimental data with statistical errors, the histograms show the expected background with errors (solid lines) and the background plus the effect (dotted lines). The vertical dashed line shows the 475 MeV threshold used in the oscillation analysis. (b) Neutrino spectrum after the background subtraction. The points represent experimental data and the solid histograms show the LSND result for $\Delta m^2 = 1.0$ eV^2 and $\Delta m^2 = 0.1$ eV^2.

4.2 Possible interpretation of results

The most popular approach in the description of solar and atmospheric oscillations, as well as the LSND result, is the introduction of one or several light (with the mass 1–10 eV) sterile neutrinos (neutrinos that do not participate in weak interactions, but can mix with the three standard neutrinos). The first MiniBooNE result substantially limited several of these exotic models. For instance, the scheme with three active neutrinos and one sterile neutrino (3 active +1 sterile) does not fit into the LSND results, and it has been excluded at a statistically significant level [85]. The oscillations of five neutrinos in the $3+2$ scheme [86] describe these data, admitting the possibility of CP violation in the lepton sector in short-baseline neutrino experiments [87]. A large difference between the $\nu_\mu \to \nu_e$ and $\bar\nu_\mu \to \bar\nu_e$ transition probabilities is expected in this model, and the antineutrino transition probability may exceed the neutrino transition probability by a factor of about three. But the analysis of all the data obtained in the reactor (for energies of several MeV) and accelerator (for neutrino energies in the GeV region) short-baseline experiments, which was performed in Ref. [88], suggests that this scheme fails to satisfactorily describe the experimental data. The same also applies to three sterile neutrinos: the $3+3$ scheme does not improve the situation. Because the occurrence of oscillations was inferred from measurements with antineutrinos (LSND + the latest MiniBooNE result) and the absence of oscillations in MiniBooNE was obtained in neutrino measurements, it was hypothesized that this discrepancy was attributable to the fact that neutrinos and antineutrinos have different masses and

mixing angles [89], i.e., to CPT violation. But the squared mass difference Δm^2 obtained from precision measurements with an antineutrino beam in the KamLAND reactor experiment agrees nicely with the Δm^2 value obtained from experiments with solar neutrinos, although it is pertinent to note that the uncertainty of the solar measurements is higher and a quantitative conclusion is difficult to draw. Furthermore, the data of the Super-Kamiokande detector, which does not distinguish between atmospheric neutrinos and antineutrinos, correspond to the same value $\Delta m^2 \sim 2.5 \times 10^{-3}$ eV^2 for both neutrinos and antineutrinos [90]. Nevertheless, the introduction of sterile neutrinos with different mixing parameters for neutrinos and antineutrinos is quite consistent with the zero MiniBooNE result for neutrino oscillations and with the positive LSND signal, as well as with the MiniBooNE result for antineutrinos.

Because the MiniBooNE detector does not distinguish between photon and electron events, one of the explanations of the excess of electron events at low energies is the hypothesis of anomalous photon production in the interaction of neutrinos with nucleons [91, 92]. This idea was first advanced to explain the excess of single-photon events in the Gargamelle bubble chamber [93]; the idea was discussed in detail and applied to interpret the MiniBooNE data in Refs [94, 95]. Also considered in Ref. [95] is the possible enhancement of the decay of the $\Delta(1232)$ resonance, which is formed in neutrino–nucleus interactions, with the emission of a single photon $\Delta \to N\gamma$, in comparison with the probability expected from the data on neutral pion production. In this case, no enhancement of this channel is expected in the interaction of antineutrinos with nuclei.

Currently, the accumulation of statistics in the MiniBooNE is ongoing, and a new experiment (MicroBooNE) [96] has been proposed for studying the effect at low neutrino energies. A time projection chamber filled with liquid argon is used as the detector, which allows identifying electrons and photons and accordingly disproving or confirming this effect and determining the nature of the 'excess' at low neutrino energies.

5. Oscillation parameters and neutrino mass

The oscillation parameters (the central values and the admissible $\pm 3\sigma$ interval) resulting from several combined analyses of all solar, reactor, atmospheric, and accelerator neutrino data are as follows:

$$\begin{aligned}
&\Delta m^2_{12} = 7.65\ (7.05 - 8.34)\ [10^{-5}\ \text{eV}^2]\,,\\
&|\Delta m^2_{23}| = 2.40\ (2.07 - 2.75)\ [10^{-3}\ \text{eV}^2]\,,\\
&\sin^2\theta_{12} = 0.304\ (0.25 - 0.37)\,,\\
&\sin^2\theta_{23} = 0.50\ (0.36 - 0.67)\,,\\
&\sin^2\theta_{13} = 0.01\ (\leqslant 0.056)\,.
\end{aligned} \tag{29}$$

Minor differences in the results of the analyses performed (the references can be found in Refs [97, 98]) do not change these quantities significantly. These parameters are renewed approximately once every two years. Because the LSND result calls for a trustworthy verification, it is not included in the conventional analysis of the oscillations of three types of active neutrinos. As mentioned in Section 2, $\Delta m^2_{12} > 0$ and the sign of Δm^2_{23} is unknown.

The best limit for the electron antineutrino mass — less than 2.0 eV (95% CL) [99] — was derived from measurement of tritium beta decay in two experiments [100, 101]. A direct electron antineutrino mass measurement with the sensitivity about 0.35 eV is expected in the KArlsruhe TRItium Neutrino (KATRIN) experiment in the near future [102]. An analysis of the data obtained in the measurement of the cosmic microwave background anisotropy and the study of structures in the Universe imposes a bound on the total neutrino mass $m_{\text{tot}} = m_1 + m_2 + m_3$. The upper bound for the total mass varies within a wide range, depending on the cosmological parameters used: $m_{\text{tot}} < 0.2 - 2.5$ eV (95% CL) (see Refs [103–105]).

6. Second-generation long-baseline experiments

Prior to discussing next-generation long-baseline experiments, it is pertinent to note that the expressions for the neutrino oscillation probability given in Section 2 describe this process in the vacuum. The presence of matter changes these expressions because there is a difference in the interaction of the three types of neutrinos with matter. The ordinary matter traversed by neutrinos contains protons, neutrons, and electrons, but does not contain muons or tau leptons. As a result, electron neutrinos interact with the electrons present in matter via charged (exchange by $W^{\pm}$) and neutral (exchange by Z^0) currents, while ν_μ with the energy < 10 GeV and ν_τ with the energy < 3 TeV can interact with electrons only via neutral currents (see Section 3.3). For ν_e, this gives rise to an additional term proportional to the electron density in the interaction Lagrangian.

The probability of $\nu_\mu \to \nu_e$ oscillations in matter (for a weak effect of matter) can be parameterized as [106–108]

$$\begin{aligned}
P(\nu_\mu \to \nu_e) = {} & 4c^2_{13}s^2_{13}s^2_{23}\sin^2\frac{\Delta m^2_{13}L}{4E_\nu}\left[1 + \frac{2a}{\Delta m^2_{13}}\,(1 - 2s^2_{13})\right]\\
& + 8c^2_{13}s_{12}s_{13}s_{23}(c_{12}c_{23}\cos\delta - s_{12}s_{13}s_{23})\\
& \times \cos\frac{\Delta m^2_{23}L}{4E_\nu}\sin\frac{\Delta m^2_{13}L}{4E_\nu}\sin\frac{\Delta m^2_{12}L}{4E_\nu}\\
& - 8c^2_{13}c_{12}c_{23}s_{12}s_{13}s_{23}\sin\delta\sin\frac{\Delta m^2_{23}L}{4E_\nu}\sin\frac{\Delta m^2_{13}L}{4E_\nu}\sin\frac{\Delta m^2_{12}L}{4E_\nu}\\
& + 4s^2_{12}c^2_{13}(c^2_{13}c^2_{23} + s^2_{12}s^2_{23}s^2_{13} - 2c_{12}c_{23}s_{12}s_{23}s_{13}\cos\delta)\\
& \times \sin^2\frac{\Delta m^2_{12}L}{4E_\nu} - 8c^2_{13}s^2_{13}s^2_{23}\cos\frac{\Delta m^2_{23}L}{4E_\nu}\,\frac{aL}{4E_\nu}\\
& \times \sin\frac{\Delta m^2_{13}L}{4E_\nu}(1 - 2s^2_{13})\,,
\end{aligned} \tag{30}$$

where $s_{ij} = \sin\theta_{ij}$ and $c_{ij} = \cos\theta_{ij}$. The first term in the right-hand side of (30) defines the contribution to the $\nu_\mu \to \nu_e$ transition due to the θ_{13} angle, and the second and third terms respectively reflect the contribution of CP-even and CP-odd terms. The fourth term describes the oscillations due to the parameters θ_{12} and Δm^2_{12}. The fifth and last term accounts for the effect of matter through which the neutrino travels over a distance L,

$$a[\text{eV}^2] = 2\sqrt{2}G_F n_e E_\nu = 7.6\times 10^{-5}\rho[\text{g cm}^{-3}]\,E_\nu[\text{GeV}]\,, \tag{31}$$

where G_F is the Fermi constant, n_e is the electron density, and ρ is the density of matter traversed by the neutrino. This effect is due to the following fact: in their passage through matter consisting of nucleons (quarks) and electrons, the electron neutrinos (unlike the muon and tau neutrinos) may experience small-angle elastic scattering on electrons of the medium

via a charged current without a change in momentum. In this case, an additional contribution to the scattering amplitude emerges, which leads to a change in probability, in comparison with that in the vacuum. In long-baseline experiments in which neutrinos pass through matter inside Earth, the quantity a is constant with a high precision (if the neutrinos do not traverse different regions of Earth: the crust, the mantle, the core). In the Sun, the electron density decreases approximately exponentially from the center to the surface, which leads to a resonance enhancement of oscillations in matter for a certain density — the Mikheev–Smirnov–Wolfenstein effect [109–112].

The probability $P(\bar{\nu}_\mu \to \bar{\nu}_e)$ follows from expression (30) by the substitution $a \to -a$, $\delta \to -\delta$ because two terms (the CP-odd one and the term related to the matter effect) have opposite signs for neutrinos and antineutrinos. As can be seen from (30), the contribution to the oscillation probability from the effect of matter is proportional to the neutrino energy; and hence the lower the neutrino energy is, the weaker the influence of matter on the oscillation probability. If the effect of matter is neglected, the CP-odd asymmetry is given by

$$A_{CP} = \frac{P(\nu_\mu \to \nu_e) - P(\bar{\nu}_\mu \to \bar{\nu}_e)}{P(\nu_\mu \to \nu_e) + P(\bar{\nu}_\mu \to \bar{\nu}_e)} \simeq \frac{\Delta m_{12}^2 L}{4E_\nu} \frac{\sin 2\theta_{12}}{\sin \theta_{13}} \sin\delta\,. \tag{32}$$

It is noteworthy that the CP violation effect is proportional to $1/\sin\theta_{13}$ and $P(\nu_\mu \to \nu_e) \sim \sin^2 2\theta_{13}$.

Figure 11 shows the dependence of different terms in (30) on the length of the experiment baseline for the neutrino energy 1 GeV. Two baselines are given, which are characteristic of oscillations of solar neutrinos with $\Delta m^2 \sim 7 \times 10^{-5}$ eV^2 (Fig. 11a) and atmospheric neutrinos with $\Delta m^2 \sim 2.5 \times 10^{-3}$ eV^2 (Fig. 11b). The probability $P(\nu_\mu \to \nu_e)$ depends on θ_{13}, θ_{23}, δ, and on the neutrino mass hierarchy, which allows simultaneously measuring several neutrino parameters in a long-baseline experiment.

On the other hand, there is a fundamental problem of separating the contributions of these parameters to the effect and then extracting the values of these parameters. Even in the case of a precision measurement of $P(\nu_\mu \to \nu_e)$ in a long-baseline accelerator experiment, there are considerable uncertainties in the value of θ_{13} due to the unknown CP phase and the sign of Δm_{23}^2 and due to the effect of matter (for experiments with a baseline several thousand kilometers long and neutrino energies of several GeV). This requires identifying and measuring the contribution of each term (see Fig. 11) to the $\nu_\mu \to \nu_e$ oscillation probability. An important part in the solution of this problem is assigned to Double Chooz [114] and Daya Bay [115] short-baseline reactor experiments, which are capable of performing pure θ_{13} measurements in a disappearance experiment, because the probability $P(\bar{\nu}_e \to \bar{\nu}_e)$ of a reactor neutrino disappearance is independent of δ, Δm_{23}^2, and the matter effect; as can be seen from (6), this probability is related to θ_{13} as

$$\begin{aligned} P(\bar{\nu}_e \to \bar{\nu}_e) &= 1 - 4\sum_{k>j} |U_{ej}|^2 |U_{ek}|^2 \sin^2 \frac{\Delta m_{jk}^2 L}{4E_\nu} \\ &= 1 - \sin^2 2\theta_{13} \sin^2 \frac{\Delta m_{13}^2 L}{4E_\nu} \\ &\quad - \frac{1}{2}\cos^2\theta_{12} \sin^2 2\theta_{13} \sin \frac{\Delta m_{13}^2 L}{2E_\nu} \sin \frac{\Delta m_{12}^2 L}{2E_\nu} \\ &\quad - \left(\cos^4\theta_{13} \sin^2 2\theta_{12} + \cos^2\theta_{12} \sin^2 2\theta_{13} \cos \frac{\Delta m_{13}^2 L}{2E_\nu}\right) \\ &\quad \times \sin^2 \frac{\Delta m_{12}^2 L}{4E_\nu}\,. \end{aligned} \tag{33}$$

Measurement of θ_{13} is the first step in the search for CP violation in the lepton sector and in the determination of neutrino mass hierarchy, because the CP violation effect always manifests itself in the product of δ and $\sin^2 2\theta_{13}$. Only a value of the angle θ_{13} that is nonzero and not too small opens a window for a sensitive search for CP violation in long-baseline accelerator oscillation experiments.

What are the theoretical predictions for the θ_{13} value? Extensions of the Standard Model that take a nonzero neutrino mass into account do not provide unique predictions for θ_{13}: its value may be close to the present-day limit, may be very small, or may even be zero. Prior to the experimental discovery of neutrino mixing, the mixing of neutrinos of different flavors was expected to be similar to the mixing of quarks, which is characterized by small angles. But the amazing result for two mixing angles, $\theta_{23} \simeq 42^\circ$ and $\theta_{12} \simeq 35^\circ$, which are substantially different from the mixing

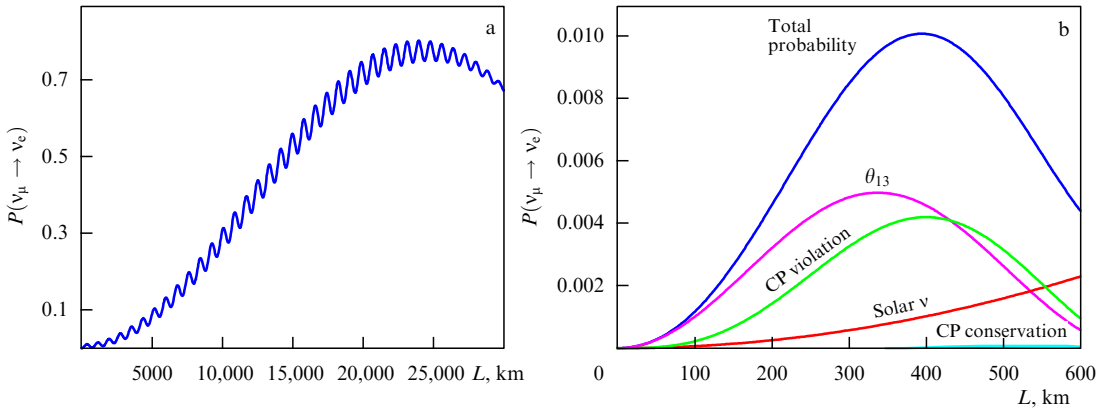

Figure 11. Dependence of $P(\nu_\mu \to \nu_e)$ on the length of the experiment baseline calculated using expression (30) for a monochromatic 1 GeV neutrino beam [113]. (a) Distances from the detector corresponding to maximum solar neutrino oscillations. (b) Characteristic distances for atmospheric neutrino oscillations: shown are the first local oscillation maximum in figure (a) and the contributions of different processes to this maximum. In both cases, the following oscillation parameters were used: $\sin^2 2\theta_{13} = 0.01$, $\sin^2 2\theta_{12} = 0.8$, $\Delta m_{23}^2 = 2.5 \times 10^{-3}$ eV^2, and $\Delta m_{12}^2 = 7.0 \times 10^{-5}$ eV^2. The CP-odd phase is respectively equal to 0 and $-\pi/2$ for figures a and b.

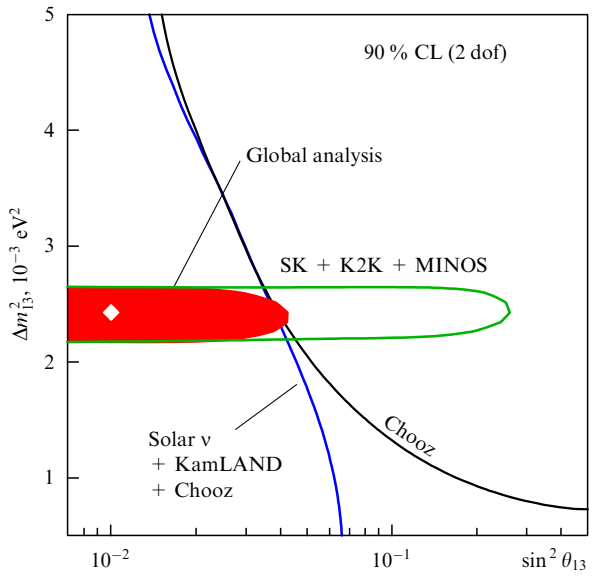

Figure 12. Bounds on $\sin^2\theta_{13}$ obtained in the analysis of all data on neutrino oscillations in solar, atmospheric, reactor, and accelerator experiments [98] (dof: degrees of freedom).

angles for quarks, indicate that there are no reasonable grounds to assume that the value of θ_{13} is very small. There is a wide class of theoretical models in which the value of θ_{13} is close to the present-day experimental limit. A broad spectrum of different model predictions for θ_{13} is given in Refs [116–118] and [119]. Figure 12 shows the experimental bound on the value of $\sin^2\theta_{13}$ obtained in Ref. [98] in the analysis of all experimental data on neutrino oscillations. Interestingly, in several recent analyses of well-known oscillation data, indications have been obtained that the value of θ_{13} is nonzero. The results are discussed in detail in Ref. [120].

6.1 T2K experiment

Only four out of six parameters that characterize neutrino oscillations (three mixing angles, two independent squared mass differences, and the CP-odd phase) have been measured to date. Furthermore, the sign of Δm^2_{23} is unknown. Measurement of θ_{13} and determination of the sign of Δm^2_{23} are the priorities for next-generation long-baseline experiments. Discovering CP violations in the neutrino sector and measuring the phase δ are the most important tasks. Improving the precision of measurement of the mixing angles is also fundamentally important. For instance, if the θ_{23} value is close to the maximal one and $\theta_{13} \sim 0$, this may be a manifestation of some new symmetry, which would call for a more fundamental theory. This problem is discussed in detail in review [121].

The main goal of the T2K second-generation long-baseline experiment [27] is the sensitive search for $\nu_\mu \to \nu_e$ oscillations and the θ_{13} angle measurement, as well as the precision measurement of other oscillation parameters. The concept, facility, expected results, and status of the experiment are outlined below.

6.1.1 Neutrino beam. *Quasimonoenergetic* (*off-axis*) *neutrino beam*. For the first time, the T2K experiment will use a quasimonoenergetic neutrino beam whose energy is tuned to the first oscillation maximum. The main properties of this beam are discussed below.

Under the assumption that the neutrino mass is negligible, in the pion rest frame, the energy and momentum of a muon neutrino resulting from the $\pi^+ \to \mu^+\nu_\mu$ decay are given by

$$E_\nu^{\rm cm} = p_\nu^{\rm cm} = \frac{m_\pi}{2}\left(1 - \frac{m_\mu^2}{m_\pi^2}\right). \tag{34}$$

We consider the case where a pion with an energy E_π travels along the z axis in the laboratory frame. Then the neutrino energy is expressed in this frame as

$$E_\nu = \gamma\left(E_\nu^{\rm cm} + \frac{p_\pi p_z^{\rm cm}}{E_\pi}\right) = \frac{E_\nu^{\rm cm}}{\gamma[1 - (p_\pi/E_\pi)\cos\theta]}, \tag{35}$$

where $p_z^{\rm cm} = p_\nu \cos\theta$ is the neutrino momentum component along the z axis in the center-of-mass system, $\gamma = E_\pi/m_\pi$, and θ is the angle between the neutrino momentum and the z axis. Using (34) and (35), we obtain an approximate expression for the neutrino energy in the laboratory frame for a small θ angle:

$$E_\nu \simeq \left(1 - \frac{m_\mu^2}{m_\pi^2}\right)\frac{E_\pi}{1 + \gamma^2\theta^2}. \tag{36}$$

It follows from (36) that at $\theta = 0$, the neutrino energy is proportional to the pion energy, which results in a broad range of neutrino beam energies when the pion energy spectrum also has a broad energy range. Differentiating expression (36) with respect to E_π, we obtain

$$\frac{{\rm d}E_\nu}{{\rm d}E_\pi} \simeq \left(1 - \frac{m_\mu^2}{m_\pi^2}\right)\frac{1 - \gamma^2\theta^2}{(1 + \gamma^2\theta^2)^2}. \tag{37}$$

Hence, the neutrino energy is weakly dependent on the pion energy for a small angle θ. In the case where $\theta = \gamma^{-1} = m_\pi/E_\pi$, the neutrino energy is completely independent of the pion energy:

$$E_\nu \approx \left(1 - \frac{m_\mu^2}{m_\pi^2}\right)\frac{m_\pi}{2\theta} \approx \frac{29.8\ {\rm MeV}}{\theta}, \tag{38}$$

i.e., for $\theta \approx m_\pi/E_\pi$, the resultant beam is practically monochromatic.

In the laboratory frame, for small angles between the pion and neutrino momenta, the neutrino flux per unit area of the detector located at a distance r from the $\pi^+ \to \mu^+\nu$ decay point is given by

$$\Phi = \left(\frac{2\gamma}{1 + \gamma^2\theta^2}\right)^2 \frac{1}{4\pi r^2}. \tag{39}$$

For all energies of the produced mesons (pions or kaons), the maximum intensity of neutrino flux is reached at $\theta = 0$. Various accelerator-produced neutrino beams and their properties are considered at length in review [122].

The idea of a monochromatic (off-axis) neutrino beam was first proposed for the E-889 experiment at the Brookhaven National Laboratory (BNL), USA [123]. A special feature of this approach is that the neutrino beam axis is not directed at the far detector. This permits tuning the neutrino beam energy to the oscillation maximum and obtaining a rather 'pure' beam of muon neutrinos with a small admixture of electron neutrinos. The intensity of the muon neutrino flux in a narrow energy interval tuned to the oscillation maximum

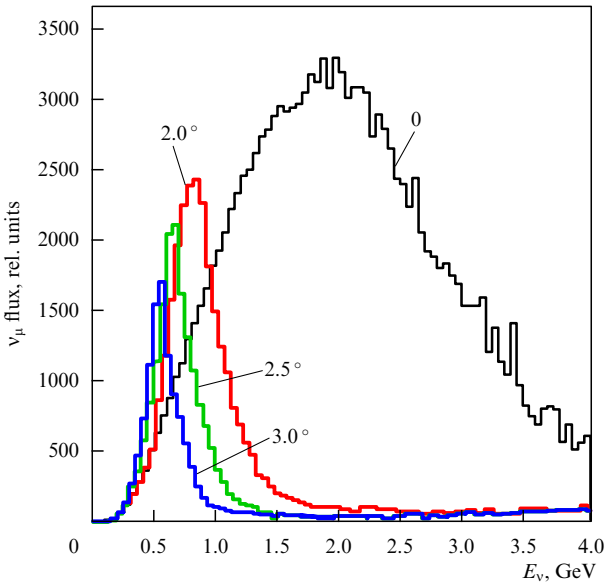

Figure 13. Neutrino spectra for different angles relative to the proton beam axis: 0, 2.0, 2.5, and 3.0 degrees. The T2K experiment uses the beam at the angle 2.5°. The neutrino beam intensity is given in arbitrary units.

by selecting the angle relative to the direction of the proton beam is also higher than the neutrino beam intensity at $\theta = 0$.

This off-axis beam concept was adopted for the T2K experiment, which uses the high-intensity proton beam of the 30 GeV proton synchrotron Japan Proton Accelerator Research Complex (J-PARC). The designed beam power is 0.75 MW, which affords the proton beam intensity of 3.3×10^{14} protons per pulse for the pulse duration about 3.0 μs and a fast beam extraction and its delivery to the target every 3.5 s. The experiment uses a graphite target 30 mm in diameter and 900 mm in length (≈ 2 nuclear paths), in which about 80% of the protons participate in nuclear interactions. The target is cooled by gaseous helium. Three toroidal pulsed magnets focus the generated pions into the 94 m long decay volume, which is filled with helium at the pressure 1 tm to reduce pion absorption and production.

The spectra of muon neutrinos calculated for several θ angles are shown in Fig. 13. The basic version of the experiment corresponds to the angle 2.5°, which can be varied between 2.0° and 3.0°, which allows changing the average neutrino energy from 0.5 to 0.9 GeV and optimizing the experimental sensitivity to the oscillation parameters [124]. For neutrino energies corresponding to the intensity maximum, the admixture of electron neutrinos from the $\pi \to \mu \to e$ decay chain and the decay of kaons is about 0.4% for the angle 2.5°. It is noteworthy that the off-axis neutrino beam parameters, which depend strongly on the angle, as is clear from Fig. 13, should be carefully monitored in the course of the experiment.

The layout of the experiment is shown in Fig. 14. The main elements of the experiment are the neutrino channel, the complex of near neutrino detectors (ND280) located 280 m away from the target, and the far Super-Kamiokande detector located at the distance of 295 km from the target. ND280 consists of two neutrino detectors and is used for measuring the parameters of the initial (prior to oscillations) neutrino beam, continuously monitoring its properties, and measuring the neutrino–nucleus interaction cross sections. One detector (the neutrino beam monitor) is located on the beam axis, i.e., at a zero angle to the direction of the proton beam; the other, the off-axis neutrino detector [125–127], is located on the axis connecting the decay volume and the SK detector, i.e., at the angle 2.5°.

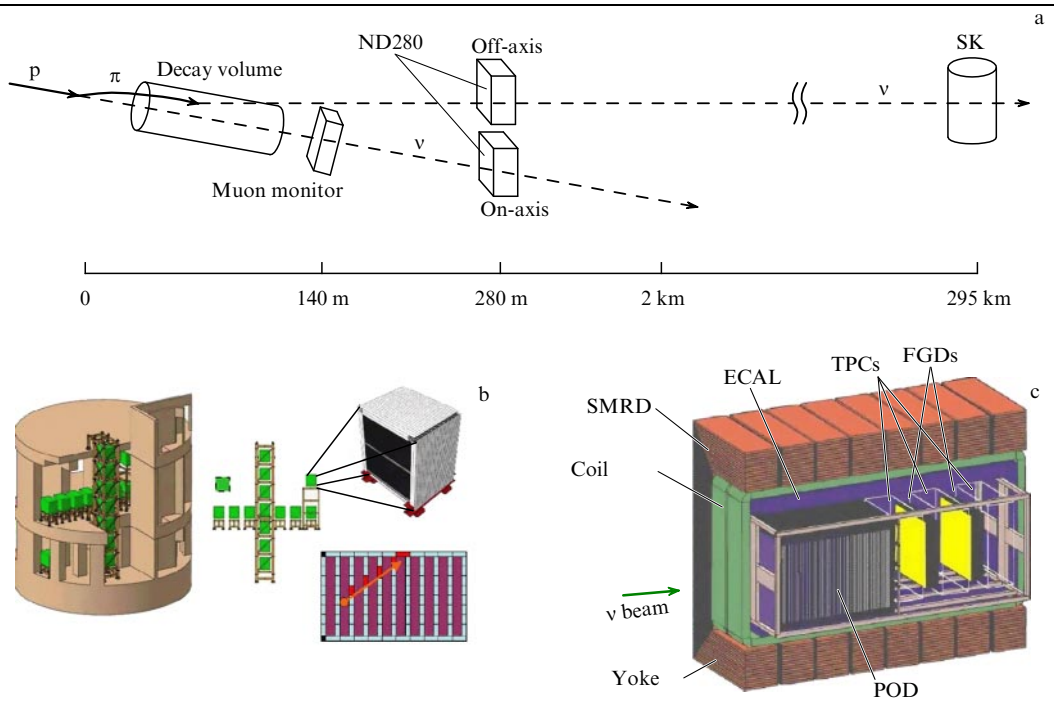

Figure 14. Layout of the T2K experiment. (a) Main elements of the facility: neutrino beam, neutrino beam monitor, near neutrino detector located 280 m away from the target, and the Super-Kamiokande far neutrino detector. (b) General view of the on-axis neutrino beam monitor and one of 16 modules, as well as a typical quasielastic event in this detector. (c) Near off-axis neutrino detector, which comprises a neutral-pion detector (POD), an electromagnetic calorimeter (ECAL), a muon range detector (SMRD), and a tracking detector, which consists of three time-projection chambers (TPCs) and two highly segmented scintillation detectors (FGDs).

6.1.2 Near neutrino detector. To achieve the experiment goals, the near neutrino detector must measure the neutrino spectrum near the target with an accuracy of 2%. To measure the neutrino energy with this accuracy, the spectrum of muons from the quasielastic neutrino scattering should be measured with the momentum resolution $\Delta p/p \leqslant 10\%$ and the absolute scale of the muon momentum should be determined with a precision better than 2%. Furthermore, the detector should have a low proton detection threshold (≈ 200 MeV/c). The admixture of electron neutrinos to the muon neutrino spectrum has to be measured with the accuracy $\approx 10\%$. One of the main detector tasks also involves the measurement of neutrino cross sections on nucleons and light nuclei. The principal function of the neutrino beam monitor consists in measuring the beam profile and monitoring the neutrino beam direction with an uncertainty < 1 mrad, which ensures monitoring the neutrino energy in the SK direction at the maximum of the spectrum better than 15 MeV.

Neutrino beam monitor. The monitor of the neutrino beam, the Interactive Neutrino GRID (INGRID) consists of $7 + 7$ identical modules arranged in the form of a cross and two additional modules, as shown in Fig. 14b. Each module of the transverse size 1×1 m^2 has a steel–scintillator sandwich structure and consists of 10 alternating steel layers 6.5 cm thick and of 11 scintillator planes. The active plane is made up of two scintillator layers, each being an assembly of scintillation bars measuring $5 \times 1 \times 121$ cm^3, which are arranged vertically in one layer and horizontally in the other. The scintillation bar has a central hole, with a wavelength shifting fiber inserted into it: this fiber transmits the scintillation signal to a photosensor, which is a micropixel avalanche photodiode operating in the limited Geiger mode, a Multi-Pixel Photon Counter (MPPC), developed by Hamamatsu, Japan. A description of these devices, their parameters, and the test data are given in Refs [128–131]. The total weight of the monitor is about 160 t. About 10^5 neutrino interactions per day are expected to occur in the detector for the proton beam power 0.75 MW.

Off-axis detector. The near (off-axis) neutrino detector consists of a UA1 magnet, a neutral pion detector (π^0 detector, or POD), a tracking detector, which comprises three time projection chambers (TPCs) and two highly segmented scintillation detectors (fine-grained detectors, or FGDs), an electromagnetic calorimeter (ECAL), and a side muon range detector (SMRD) (Fig. 14c). With the exception of the TPCs, scintillation detectors with wavelength shifting fibers are used for active elements in all of these detectors, with MPPCs serving as photodetectors.

The neutral pion detector is optimized for measuring the π^0 production cross section via neutral currents:

$$\nu_\mu + N \to \nu_\mu + \pi^0 + N\,, \tag{40}$$

where $N = \mathrm{n}, \mathrm{p}$. Measuring these processes plays an important role in determining the background in the measurement of the spectrum of electron neutrinos emerging in Super-Kamiokande due to $\nu_\mu \to \nu_e$ oscillations, because an event in which only one photon from the $\pi^0 \to \gamma\gamma$ decay is detected is identified as a single electron from the quasielastic scattering of an electron neutrino. The POD consists of alternating water layers, each 3 cm thick, and track planes. One track plane, in turn, consists of two XY-planes, in which scintillation plates are arranged perpendicular to each other. For the efficient detection of photons, thin brass plates are placed between the scintillation planes in the central part of the detector, and lead plates are inserted in the front and rear parts of the detector. The total POD weight is about 17 t and the water target weight is about 3 t. This mass is sufficient for collecting 10^4 π^0 produced via neutral and charged currents during the experiment execution. The cross sections for production of neutral pions in oxygen with energies $\leqslant 1$ GeV will be measured with the aid of this detector.

The tracking detector measures the flux and spectrum of muon and electron neutrinos by detecting charged leptons produced in quasielastic neutrino scattering. The main process for T2K energies is the quasielastic scattering via a charged current:

$$\nu_\mu + \mathrm{n} \to \mu^- + \mathrm{p}\,. \tag{41}$$

Precisely measuring the neutrino spectrum requires detecting and reconstructing the kinematic parameters of both the muon and the proton. The proton is identified and measured by the FGDs, and the muon momentum is measured by the TPC with the addition of information from the FGD. The neutrino energy will be reconstructed from the value of the muon momentum.

The first FGD is a full-active scintillation detector similar to the SciBar detector [49, 50]. It consists of 30 layers of scintillating bars with the cross section 1×1 cm^2, which form alternating XY-layers perpendicular to the neutrino beam direction. The second FGD contains 3 cm thick water layers between scintillator layers. The total water weight is 0.44 t. This configuration allows simultaneously measuring the cross sections for neutrino interactions in water and carbon by comparing the events in both detectors. About 4×10^5 neutrino events are expected in both FGDs during the entire period of data taking.

The time-projection chambers, which are embedded in a 0.2 T magnetic field, should provide a momentum resolution $\approx 10\%$ in the 1 GeV/c muon momentum range. An absolute calibration of the energy scale with an accuracy about 2% may result from the reconstruction of the mass of neutral kaons produced in deep-inelastic neutrino scattering. High resolution ($< 10\%$) is also expected in measuring the specific energy loss $\mathrm{d}E/\mathrm{d}x$, which will enable a reliable (at a 5σ level) identification of muons and electrons in the 0.3–1.0 GeV/c momentum range.

The tracking detectors and the POD are surrounded by an electromagnetic calorimeter whose primary function is the detection and identification of the particles that escape from the inner detectors. The calorimeter, which has an effective thickness about 10 radiation lengths, consists of alternating layers of lead and plastic scintillator, and has the energy resolution $7.5\%/\sqrt{E\,[\mathrm{GeV}]}$ for electromagnetic showers. The muons that escape from the tracking detector at large angles cannot be measured by the TPC. They enter the magnet yoke and their momentum can be measured from their range determined using the SMRD, whose active elements are scintillating plates [132, 133] inserted in the air gaps of the magnet yokes. To collect and transport the scintillation light, wavelength shifting fibers glued in S-like grooves are used, and MPPC photodiodes serve as photosensors to detect scintillation signals from both fiber ends [133].

The near neutrino detector thus configured permits carrying out measurements of the neutrino beam near the target (the spectrum and the intensity at the angles 0 and 2.5°), measuring the admixture of electron neutrinos that

Table 1. The expected number of electron neutrinos in the Super-Kamiokande detector for the exposure 5×10^{21} POT corresponding to five years of the physics run. The simulations were made using the Neutrino Interaction Simulation Program (NEUT) [135] with the oscillation parameters $\Delta m^2_{23} = 2.5 \times 10^{-3}$ eV^2 and $\sin^2 2\theta_{13} = 0.1$. FC and FV are the events in which the neutrino interaction point is inside the Super-Kamiokande fiducial volume and their energy is completely deposited in the detector.

2.5° neutrino beam	ν_μ, charged current	ν_μ, neutral current	Admixture, ν_e	Signal, ν_e
FV, FC, $E_{vis} > 100$ MeV	2215	847	184	243
Single-ring events	1043	220	88	204
e-like rings	39	175	85	202
Absence of Michel electrons	12	156	71	187
$0.35 \leqslant E_\nu^{rec} \leqslant 0.85$ GeV	1.8	47	21	146
π^0 suppression	0.7	9	13	103

arise from the decays of muons and kaons, and measuring the cross sections of neutrino interactions with nucleons and different nuclei via charged and neutral currents. Based on these measurements, predictions for the spectrum and number of muon and electron neutrinos in the far SK detector in the absence of oscillations and calculations of $R(\mathrm{F/N})$ are made.

6.1.3 Expected results and status of the experiment. To achieve the goal of measuring θ_{13}, the electrons resulting from the electron neutrino interactions in the SK detector due to charged currents should be detected efficiently. Simultaneously, production of neutral pions in the interaction of muon neutrinos with the detector material via neutral currents must be maximally suppressed.

The problem consists in the π^0 identification in the case of the asymmetric $\pi^0 \to \gamma\gamma$ decay, when one of the photons has a low energy, resulting in the actuation of a small number of PMTs in the SK, and identification of the Cherenkov ring of this photon is hindered. Fortunately, these events are quite rare, and the number of events with a missed ring can be determined rather accurately because the decay kinematics are well known.

Table 1 shows the criteria that will be used in T2K to suppress the background processes and the efficiency expected for detection of the electron neutrino signal [134]. The first line gives the number of events for the expected signal assuming that $\sin^2 2\theta_{13} = 0.1$ (the right column) and for the main background processes, which include the events occurring via charged and neutral currents from muon neutrinos and events from the admixture of electron neutrinos in the beam for the designed J-PARC proton beam intensity and the five-year accumulation of statistics. The only criterion is the constraint that the reconstructed event energy be higher than 100 MeV. The numbers of single-ring events are shown in the second line. The third line shows the number of events in each column that satisfy the condition that a single-ring event looks like an e-like event and a delayed electron signal from the decay of a muon produced in neutrino interaction is absent. As is clear from Table 1, this condition suppresses muon neutrino quasielastic events almost completely. The next criterion imposes the condition that the neutrino energy is close to the oscillation maximum. The background events with a broader distribution in energy are thereby suppressed. Under these conditions, a substantial decrease is expected in the level of background events, while a rather high (about 42%) efficiency for the expected signal is preserved. An interesting feature is a substantial decrease in the contribution of electron neutrinos to the expected signal. This is attributable to the fact that the electron neutrinos in the initial beam have higher energies than those of the electron neutrinos produced as a result of oscillations.

The expected sensitivity to the θ_{13} angle, based on the data in Table 1, is shown in Fig. 15 for three possible systematic errors: 5%, 10%, and 20% [136]. Figure 15a shows how the sensitivity of θ_{13} measurement depends on the CP-odd phase and Fig. 15b shows the dependence of $\sin^2 2\theta_{13}$ on Δm^2_{23} under the assumption that $\delta = 0$. Also shown is the parameter region excluded in the Chooz experiment. Another important goal of the T2K experiment is the measurement of the known oscillation parameters to within $\delta(\Delta m^2_{23}) \sim 10^{-4}$ eV^2 and $\delta(\sin^2 2\theta_{23}) = 0.01$ using the methods developed by K2K for the analysis of the deficit and spectrum shape distortion of muon neutrinos in Super-Kamiokande.

Status of the experiment. The construction of the J-PARC accelerator facility was completed in 2008. In April 2009, the proton beam was injected into the neutrino channel and the muon monitor (MUMON) detected the muon signal from a $\pi \to \mu + \nu$ decay. ND280 detected the first neutrino events in November 2009. The physical run began in January 2010 for the proton energy 30 GeV, and the first neutrino event in Super-Kamiokande was detected in February 2010. The proximate experiment goal is to collect the integral luminosity equal to (2.0–2.5) $\times 10^{20}$ POT, which is expected to allow obtaining the sensitivity of $\sin^2 2\theta_{13}$ exceeding the Chooz limit by a factor of about 2.5 already in 2011.

6.2 NOvA experiment

As discussed above, for a sufficiently long baseline, accelerator experiments are sensitive to δ and the mass hierarchy, while reactor experiments with the baseline about 1 km, which are insensitive to these parameters, enable 'pure' measurements of θ_{13}, without unraveling the intricate picture of correlations of the oscillation parameters. If the $\nu_\mu \to \nu_e$ oscillations are discovered in the T2K accelerator experiment and the $\bar\nu_e \to \bar\nu_e$ oscillations are observed in Double Chooz and Daya Bay reactor experiments, the combination of these data will permit bounding the region for the CP-odd phase and will open the way to determine the neutrino mass hierarchy in the NOvA long-baseline accelerator experiment.

The NOvA experiment proposed at Fermilab, aimed at the investigation of $\nu_\mu \to \nu_e$ and $\bar\nu_\mu \to \bar\nu_e$ oscillations with the sensitivity $\approx 1\%$ to the transition probabilities for both processes, has been scientifically approved and is now in the stage of detector construction. The experiment will use a 2.5° off-axis beam of muon neutrinos and antineutrinos with the average energy 2 GeV, as well as two neutrino detectors, a near detector and a far one. If $\theta_{13} \neq 0$, determining the

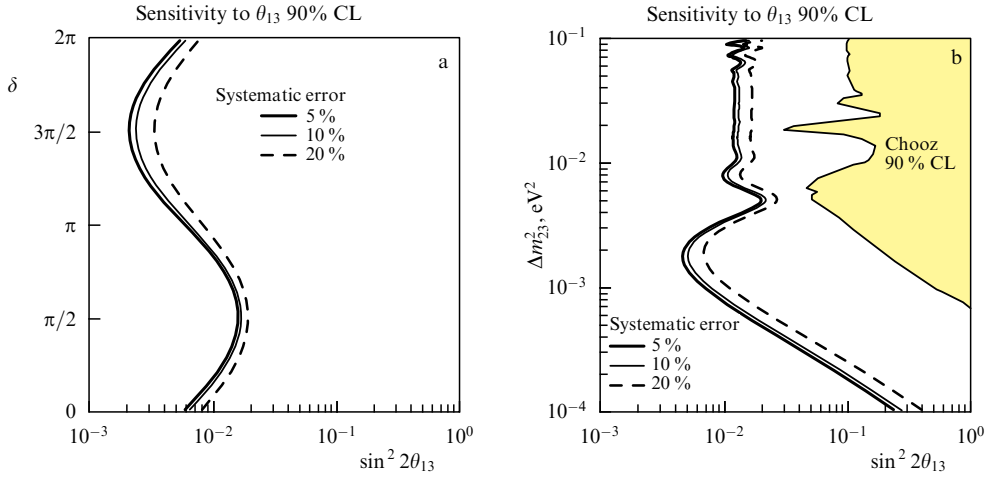

Figure 15. The T2K experiment sensitivity to the θ_{13} angle (90% CL) for 5 years of statistics collection for the proton beam power 750 kW and the super-Kamiokande volume 22.5 kt [136]. (a) Dependence of θ_{13} on δ is shown for the systematic errors 5%, 10%, and 20%. The oscillation parameters are $\sin^2 2\theta_{12} = 0.87$, $\sin^2 2\theta_{23} = 1.0$, $\Delta m^2_{12} = 7.6 \times 10^{-5}$ eV^2, and $\Delta m^2_{23} = 2.4 \times 10^{-3}$ eV^2. (b) Dependence of θ_{13} on Δm^2_{23} for three systematic errors: 5%, 10%, and 20%. The oscillation parameters are $\sin^2 2\theta_{12} = 0.87$, $\sin^2 2\theta_{23} = 1.0$, $\Delta m^2_{12} = 7.6 \times 10^{-5}$ eV^2, $\Delta m^2_{23} = 2.4 \times 10^{-3}$ eV^2, and $\delta = 0$. Also shown (in grey) is the domain excluded at a level of 90% CL in the Chooz experiment.

neutrino mass hierarchy will become the primary task of the experiment.

6.2.1 Near and far detectors. Both detectors, near and far, will be fully active segmented scintillation detectors. A small neutrino detector, which is an exact replica of the far one, will be located approximately 1 km away from the target and the far detector approximately 810 km away from the target and 12 km away from the beam axis. The mass of the near detector will be about 215 t and the mass of the far detector about 15 kt. The main element of both detectors is a plastic cell measuring 3.8 cm transversely to the beam and 5.9 cm along the beam direction; the cell is filled with a liquid scintillator, with a wavelength-shifting fiber placed in it for transporting the scintillation light to the photodetector. Each cell is 15.6 m long in the far detector and 2.9 (4.2) m long in the near detector for the horizontal (vertical) planes.

Both detectors are structurally similar and have alternating layers in which the cells are arranged horizontally and vertically. The active part of the detectors (the scintillator) comprises about 70% of the total detector mass. The scintillation light emerging in the cells is absorbed by U-shaped wavelength-shifting fibers 0.7 mm in diameter, reemitted, and transported to both ends, where it is detected by avalanche photodiodes. The total fiber length in a cell of the far detector is about 34 m. For a relativistic particle, the use of avalanche photodiodes, which have a high quantum efficiency, enables obtaining a specific yield of 20 photoelectrons from the far end of the cell, where the fiber is bent. The light yield averaged over the whole cell length is expected to be 28 photoelectrons. The far detector has the size $15.6 \times 15.6 \times 78$ m^3 and the near one the size $4.2 \times 2.9 \times 14.3$ m^3. The structure of both detectors (Fig. 16), which is optimized for detecting electron neutrinos, permits discriminating between muon and electron events. The simulated tracks of muons and electrons produced by muon and electron neutrinos via charged currents are nicely distinguished in the detector: the electron track has a diffuse profile and the muon track is a straight line.

6.2.2 Expected experiment sensitivity. NOvA has the capacity to perform measurements with both a beam of muon neutrinos and a beam of muon antineutrinos. At the first stage of the experiment, measurements will be carried out for the proton beam energy 120 GeV and the power 700 kW. Subsequently, the power will be increased to 1.2 MW. The estimates of experiment sensitivity given below were made under the assumption that the beam power is equal to 1.2 MW and the accumulation of statistics is continued for three years (44 weeks per year) with neutrino and antineutrino beams.

Because the effect of matter increases (decreases) the probability of the $\nu_\mu \to \nu_e$ ($\bar\nu_\mu \to \bar\nu_e$) oscillations by 30% [see expression (30)], the possibility of determining the hierarchy of neutrino masses is very interesting. This is illustrated by Fig. 17, which shows the results for the muon-to-electron neutrino conversion probability $P(\nu_\mu \to \nu_e) = 2\%$. For instance, when the muon-to-electron antineutrino conversion probability (the abscissa) is equal to 1% or 4%, the

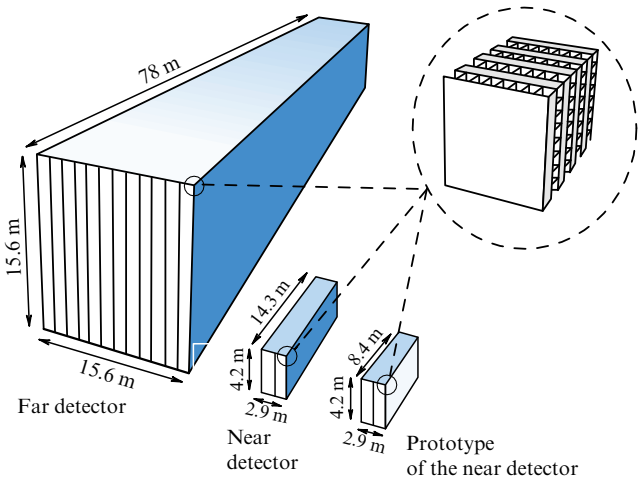

Figure 16. Schematic representation of NOvA detectors. The far detector measures $15.6 \times 15.6 \times 78$ m^3 and the near one measures $4.2 \times 2.9 \times 14.3$ m^3.

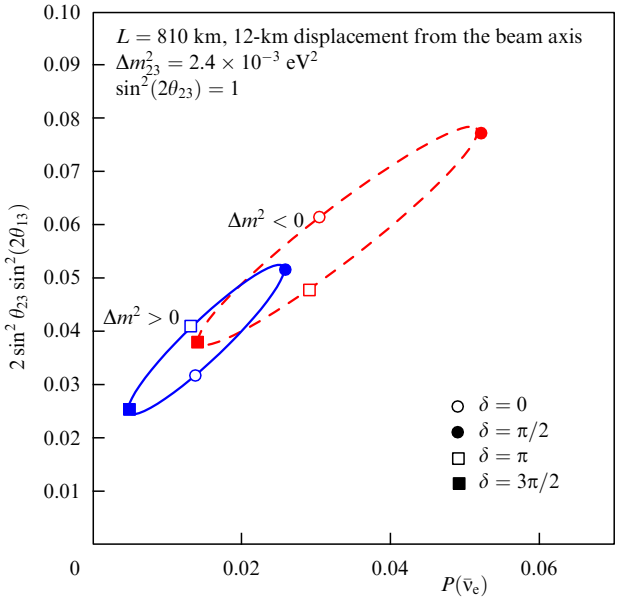

Figure 17. Possible manifestation of mass hierarchy in the NOνA experiment for a muon-to-electron neutrino oscillation probability $P(\nu_\mu \to \nu_e) = 2\%$. Plotted on the abscissa is the probability $P(\bar{\nu}_\mu \to \bar{\nu}_e)$ of muon-to-electron antineutrino oscillations. The ellipses plotted in this figure were obtained assuming zero-error measurements.

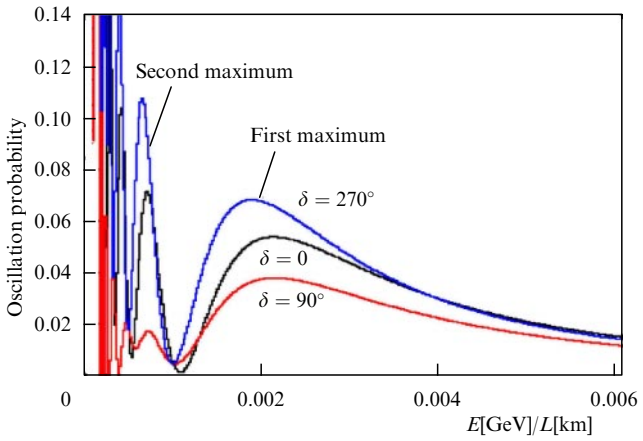

Figure 18. Dependence of the $\nu_\mu \to \nu_e$ oscillation probability on the ratio E[GeV]/L[km] for $\sin^2 2\theta_{13} = 0.1$ and three CP-odd phase values [140].

mass hierarchy may be reliably determined. But if the conversion probabilities for neutrinos and antineutrinos is about 2%, this will be impossible to achieve. Required in this case is a third measurement made in a different experiment with neutrino energies and the baseline different from those in the NOνA, or measurements with the NOνA made in the second oscillation peak.

7. Distant future

The further prospects of long-baseline accelerator experiments depend on the θ_{13} value. If this parameter is nonzero, the principal objective will be the search for CP violation in the lepton sector, which may be discovered in oscillation experiments measuring the asymmetry between the transitions of muon neutrinos and antineutrinos to electron neutrinos and antineutrinos, as well as measuring the oscillatory curve with the use of a wide neutrino energy range covering two oscillation maxima [137, 138].

One realistic scenario involves an increase in the J-PARC proton beam power to ≈ 1.7 MW and the execution of an experiment with two (or even three) far detectors located in Kamioka (295 km away from J-PARC) on Okinosima Island (660 km, the off-axis angle $\approx 0.8°$) and/or in Korea (1050 km, the off-axis angle $\approx 1.0°$) [139, 140]. A water Cherenkov detector and large liquid-argon TPCs are being considered for detectors. This configuration would allow carrying out measurements with a neutrino beam simultaneously in the first and second peaks of $\nu_\mu \to \nu_e$ oscillations with good statistics.

A manifestation of CP violation (the position and intensity of the first and second oscillation peaks) is demonstrated in Fig. 18 for $\sin^2 2\theta_{13} = 0.1$ and three δ values. Carrying out these measurements requires a high-intensity neutrino beam with a broad energy spectrum. A similar approach is being considered for long-baseline neutrino experiments at Fermilab [141]. An alternative approach consists in the search for CP violation with one massive detector and high-intensity beams of muon neutrinos and antineutrinos. One possible version involves the use of two Cherenkov detectors with the total mass about 540 kt located in Kamioka 295 km away from J-PARC [142]. In this case, the energies of both beams should be tuned to the first oscillation maximum.

7.1 Beta beams and neutrino factories

The highest sensitivity to δ and other oscillation parameters may be attained in experiments with next-generation high-intensity neutrino beams. Unlike the approaches using conventional neutrino beams that are obtained from the decays of pions produced in proton–nuclear collisions, the approaches whereby neutrino beams are formed in the decays of radioactive nuclei (beta beams [143]) and muons (neutrino factory [144]) are radically new.

7.1.1 Beta beams. When a nucleus experiences a beta decay, an electron neutrino or antineutrino is emitted. In the rest frame of the nucleus, the neutrinos are emitted isotropically. In the case of an accelerated ion, a collimated neutrino beam is formed. The idea of a beta beam [143] is that accelerated radioactive nuclei that experience β decay are the sources of pure ν_e and $\bar{\nu}_e$, in accordance with the type of accelerated nucleus. Presumably, the best radioactive ions for electron neutrino beams are the nuclei ^{18}Ne ($^{18}_{10}\mathrm{Ne} \to {}^{18}_{9}\mathrm{F} + e^+ + \nu_e$) and for antineutrino beams, the nuclei ^{6}He ($^6_2\mathrm{He} \to {}^6_3\mathrm{Li} + e^- + \bar{\nu}_e$). In this case, the neutrino energy depends on the ion energy and can be varied to optimize the experiment sensitivity.

A well-collimated neutrino beam consists of one type of neutrino with known energy and intensity. For a long-baseline experiment, there is no need for a near detector, because the neutrino spectrum can be specified by only two parameters: the upper limit energy of the β-spectrum and the Lorentz factor γ of decaying ions, while the neutrino flux is normalized via measurements of the number of ions circulating in the decay ring. Because the neutrino beam is free from admixtures of muon neutrinos and antineutrinos, there is no need for a detector with a magnetic field for the precision measurement of $\nu_e \to \nu_\mu$ oscillations to obtain information on θ_{13} and δ.

Several versions of beta beams are presently under discussion. Depending on the value of γ, they are classified

into low-energy ($\gamma = 6-15$), intermediate-energy ($\gamma \geqslant 100$), and high-energy ($\gamma \sim 1000$) beams. These concepts were considered in detail in Ref. [145]. The neutrino and antineutrino flux intensities in low-γ beta beams may amount to $\sim 10^{18}$ ν_e per year with acceleration of ^{18}Ne, and to $\sim 3 \times 10^{18}$ $\bar{\nu}_e$ per year with acceleration of ^{6}He [146, 147].

A beta beam can be produced on the basis of a high-intensity source of radioactive ions with the use of the Proton Synchrotron (PS) and Super Proton Synchrotron (SPS) proton accelerators at CERN (Fig. 19a). The high-intensity proton beam accelerated to the energy 2.2 GeV in the superconducting linear proton accelerator (Superconducting Proton Linac, SPL) is directed to the target that produces radioactive nuclei. Upon ionization, the radioactive ions are accelerated to the energy about 300 MeV per nucleon. Subsequently, due to acceleration in the PS and SPS, their energy increases to 100 GeV per nucleon and the ions are accumulated in a ring approximately 6.8 km in length. The straight decay section directed at the neutrino detector should be approximately 2.5 km long; in this case, the average neutrino beam energy is about 600 MeV and the optimal distance to the neutrino detector, at which the sensitivity to oscillations is maximal, should be about 300 km. The possibility of making the beta beam on the basis of the Fermilab accelerator facility is also being discussed [148]. The neutrino detector is to be accommodated in the Deep Underground Science and Engineering Laboratory (DUSEL) located approximately 1300 km away from the neutrino source.

7.1.2 Neutrino factories. The concept of a neutrino factory consists in the production of a high-intensity neutrino beam from the decays of muons accumulated in a storage ring with a long straight sections for decays. This concept is a natural development of the idea of the muon collider first introduced by Budker [149].

One possible version of a neutrino factory is schematically shown in Fig. 19b. The pions produced in the target bombardment by a proton beam with the power about 4 MW are efficiently collected in a decay channel with the use of a superconducting solenoid or a system of horn magnets, in which the pions decay into muons with an energy spectrum close to that of the pions. The highest-intensity part of the muon spectrum corresponds to a momentum in the range 250 ± 100 MeV/c. The muon spectrum is monochromatized by an alternating electric field, which decelerates fast muons and accelerates slow ones. Decreasing the transverse size and the angular beam divergence requires lowering the muon energy. This can be achieved by ionization cooling [150]. Essentially, the method is as follows: the muons lose their energy in passing through a low-Z substance (liquid hydrogen) embedded in a strong-focusing magnetic field. At the output of the cooling channel, the muons have the longitudinal momentum about 100 MeV/c and virtually zero transverse components. Next, the muons are accelerated in a linear accelerator to energies 20–50 GeV. Approximately 10^{21} muons per year can be collected in a storage ring, in which they on average execute several hundred turns prior to decay. In the case of a positive muon beam, the $\mu^+ \to e^+\nu_e\bar{\nu}_\mu$ decays give rise to a high-intensity $\nu_e + \bar{\nu}_\mu$ beam, and in the case of negative muons, the neutrino beam is a $\bar{\nu}_e + \nu_\mu$ mixture. The sensitivity to different oscillation parameters, including the sensitivity to the CP-odd phase, attainable at the neutrino factory, was comprehensively analyzed in Ref. [151]. For instance, the $\nu_e \to \nu_\mu$ transition probability can be measured with the sensitivity $10^{-4}-10^{-5}$, which corresponds to the $10^{-3}-10^{-4}$ range for $\sin^2 2\theta_{13}$. Different detector versions elaborated for the neutrino factory were considered at length in Ref. [152].

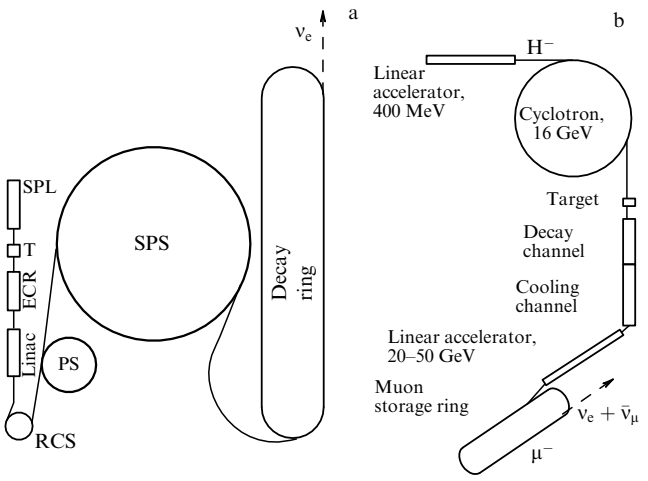

Figure 19. (a) Schematic representation of the possible accelerator setup for a beta beam at CERN. (b) Diagrammatic representation of a neutrino factory with one muon storage ring. SPL — high-intensity linear proton accelerator, T — target, ECR – electron cyclotron resonance ion source, RCS — rapid-cycling cyclotron.

8. Conclusions

Despite the brilliant results obtained during the last decade, neutrino physics faces several basic problems that remain to be solved. We list only some of them.

— What is the nature of neutrinos: Dirac or Majorana particles?

— Is the CP symmetry violated in the lepton sector?

— What are the mass hierarchy and the absolute mass scale of neutrinos?

— Why are neutrinos different from other leptons?

— What is the mechanism of neutrino mass formation?

— Why do neutrinos and quarks exhibit different mixing?

— Do sterile neutrinos exist?

We note once again that the investigation of neutrino oscillations is the study of new physics beyond the Standard Model. The immediate task of neutrino accelerator experiments is the discovery of the 'golden mode' of $\nu_\mu \to \nu_e$ oscillations and the measurement of the θ_{13} angle. The future of long-baseline experiments and the prospects of CP-violation measurement in these experiments depend to a large measure on the value of this parameter. If the θ_3 value turns out to be close to the Chooz limit, next in line are the determination of the mass hierarchy and the search for CP violation in the lepton sector. If $\sin^2 2\theta_{13} > 0.01$, the matter effect can be used for measuring the mass hierarchy; but if $\sin^2 2\theta_{13} < 0.01$, the solution of this problem will call for new approaches to detectors and accelerator technologies. If $\theta_{13} \approx 0$, the phase δ cannot be measured in long-baseline neutrino experiments.

Figure 20, based on the estimates in Ref. [153], shows the sensitivity to $\sin^2 2\theta_{13}$ expected for the ongoing accelerator and reactor experiments, as well as those under preparation or planned for the next few years.

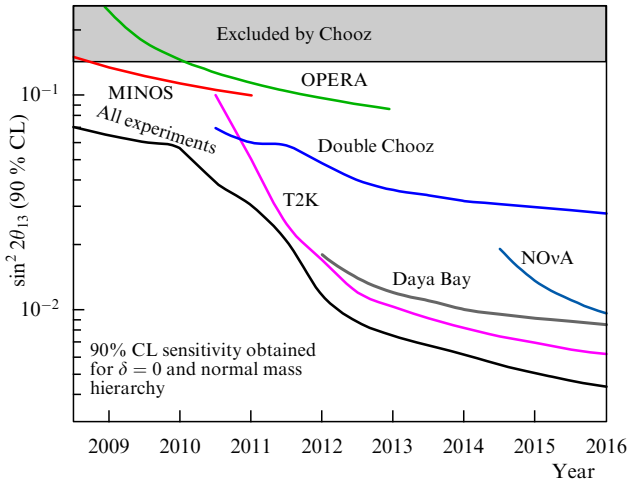

Figure 20. Sensitivity to $\sin^2 2\theta_{13}$ expected from different accelerator and reactor experiments in the next few years [153]. A value of $\Delta m^2_{23} = 2.5 \times 10^{-3}$ eV^2 was used for the estimates; furthermore, the normal mass hierarchy and $\delta = 0$ assumed for accelerator experiments.

Acknowledgments. We are thankful to L B Okun' for the idea of writing this review. It is our pleasure to express the deep gratitude to V A Matveev, V A Rubakov, and S S Gershtein for their helpful advice and interest in the work. We thank M Mezzetto, T Kobayashi, T Nakaya, D Karlen, A V Kopylov, and D S Gorbunov for the numerous fruitful discussions, important remarks, and valuable information.

This work was supported by the Neutrino Physics Program of the Presidium of the RAS, joint RFBR/JSPS (Japan) grant No. 08-02-91206-YaF-a, and the Program for Support of Scientific Schools (NSh-4918.2008.2, NSh-65038.2010.2).

References

1. Pontecorvo B M *Zh. Eksp. Teor. Fiz.* **33** 549 (1957) [*Sov. Phys. JETP* **6** 429 (1957)]
2. Pontecorvo B M *Zh. Eksp. Teor. Fiz.* **34** 247 (1957) [*Sov. Phys. JETP* **7** 172 (1958)]
3. Pontecorvo B M *Zh. Eksp. Teor. Fiz.* **53** 1717 (1967) [*Sov. Phys. JETP* **26** 984 (1967)]
4. Gribov V, Pontecorvo B *Phys. Lett. B* **28** 493 (1969)
5. Davis R (Jr.), Harmer D S, Hoffman K C *Phys. Rev. Lett.* **20** 1205 (1968)
6. Bahcall J N *Neutrino Astrophysics* (Cambridge: Cambridge Univ. Press, 1989)
7. Hirata K S (Kamiokande Collab.) *Phys. Rev. Lett.* **65** 1297 (1990)
8. Hirata K S (Kamiokande Collab.) *Phys. Rev. D* **44** 2241 (1991); "Erratum" *Phys. Rev. D* **45** 2170 (1992)
9. Fukuda Y et al. (Kamiokande Collab.) *Phys. Rev. Lett.* **77** 1683 (1996)
10. Fukuda Y et al. (Super-Kamiokande Collab.) *Phys. Rev. Lett.* **81** 1158 (1998)
11. Abdurashitov J N et al. (SAGE Collab.) *Phys. Lett. B* **328** 234 (1994)
12. Anselmann P et al. (GALLEX Collab.) *Phys. Lett. B* **285** 376 (1992)
13. Ahmed S N et al. (SNO Collab.) *Phys. Rev. Lett.* **92** 181301 (2004)
14. Eguchi K et al. (KamLAND Collab.) *Phys. Rev. Lett.* **90** 021802 (2003)
15. Fukuda Y et al. (Super-Kamiokande Collab.) *Phys. Rev. Lett.* **81** 1562 (1998)
16. Aliu E et al. (K2K Collab.) *Phys. Rev. Lett.* **94** 081802 (2005)
17. Michael D G et al. (MINOS Collab.) *Phys. Rev. Lett.* **97** 191801 (2006)
18. Ashie Y et al. (Super-Kamiokande Collab.) *Phys. Rev. Lett.* **93** 101801 (2004)
19. Dolgov A D *Phys. Rep.* **370** 333 (2002)
20. Dolgov A D *ЯФ* **71** 2189 (2008) [*Phys. Atom. Nucl.* **71** 2152 (2008)]; arXiv:0802.2887
21. Otten E W, Weinheimer C *Rep. Prog. Phys.* **71** 086201 (2008)
22. Barabash A S *Yad. Fiz.* **70** 1230 (2007)
23. Kota V K B, Sarkar U, in *Neutrinoless Double Beta Decay* (Eds V K B Kota, U Sarkar) (New Delhi: Narosa Publ. House, 2008) p. 164
24. Zuber K, arXiv:1002.4313
25. Guler M et al. (OPERA Collab.), CERN-SPSC-2000-028
26. Declais Y et al., CERN-SPSC-2002-029 SPSC-059
27. Itow Y et al., hep-ex/0106019
28. Ayres D et al. (NOvA Collab.), hep-ex/0210005; hep-ex/0503053
29. Aguilar-Arevalo A A et al. (MiniBooNE Collab.) *Phys. Rev. Lett.* **98** 231801 (2007)
30. Aguilar A et al. (LSND Collab.) *Phys. Rev. D* **64** 112007 (2001)
31. Gershtein S S, Kuznetsov E P, Ryabov V A *Usp. Fiz. Nauk* **167** 811 (1997) [*Phys. Usp.* **40** 773 (1997)]
32. Ryabov V A *Fiz. Elem. Chastits i At. Yadra* **34** 1256 (2003) [*Phys. Part. Nucl.* **34** 651 (2003)]
33. Dore U, Orestano D *Rep. Prog. Phys.* **71** 106201 (2008)
34. Kudenko Yu G *Yad. Fiz.* **72** 537 (2009) [*Phys. At. Nucl.* **72** 501 (2009)]
35. Hernandez P, arXiv:1010.4131
36. Maki Z, Nakagawa M, Sakata S *Prog. Theor. Phys.* **28** 870 (1962)
37. Apollonio M et al. (Chooz Collab.) *Phys. Lett. B* **466** 415 (1999)
38. Roy D P *Phys. News India* **39** (3) 51 (2009); arXiv:0809.1767
39. Giunti C, Kim Ch W *Fundamentals of Neutrino Physics and Astrophysics* (Oxford: Oxford Univ. Press, 2007)
40. Mohapatra R N et al. *Rep. Prog. Phys.* **70** 1757 (2007); hep-ph/0510213
41. de Gouvea A, arXiv:0902.4656
42. Fogli G L et al. *Prog. Part. Nucl. Phys.* **57** 742 (2006); hep-ph/0506083
43. Barger V, Marfatia D, Whisnant K *Phys. Rev. D* **65** 073023 (2002); hep-ph/0112119
44. Ahn M H et al. (K2K Collab.) *Phys. Rev. Lett.* **90** 041801 (2003); hep-ex/0212007
45. Fukuda S et al. (Super-Kamiokande Collab.) *Nucl. Instrum. Meth. Phys. Res. A* **501** 418 (2003)
46. Kasuga S et al. *Phys. Lett. B* **374** 238 (1996)
47. Suzuki A et al. (K2K Collab.) *Nucl. Instrum. Meth. Phys. Res. A* **453** 165 (2000)
48. Kim B J et al. *Nucl. Instrum. Meth. Phys. Res. A* **497** 450 (2003)
49. Nitta K et al. *Nucl. Instrum. Meth. Phys. Res. A* **535** 147 (2004)
50. Yamamoto S et al. *IEEE Trans. Nucl. Sci.* **52** 2992 (2005)
51. Berns H C, Wilkes R J *IEEE Trans. Nucl. Sci.* **47** 340 (2000)
52. Catanesi M G et al. (HARP Collab.) *Nucl. Phys. B* **732** 1 (2006)
53. Cho Y et al. *Phys. Rev. D* **4** 1967 (1971)
54. Ahn M H et al. (K2K Collab.) *Phys. Rev. D* **74** 072003 (2006)
55. Michael D G et al. (MINOS Collab.) *Nucl. Instrum. Meth. Phys. Res. A* **596** 190 (2008); arXiv:0805.3170
56. Adamson P et al. (MINOS Collab.) *Phys. Rev. D* **77** 072002 (2008)
57. Adamson P et al. (MINOS Collab.) *Phys. Rev. Lett.* **101** 131802 (2008); arXiv:0806.2237
58. Barger V et al. *Phys. Rev. Lett.* **82** 2640 (1999)
59. Fogli G L et al. *Phys. Rev. D* **67** 093006 (2003)
60. Vahle P, talk at *24th Intern. Conf. on Neutrino Physics and Astrophysics*: *NEUTRINO2010, Athens, Greece, 14 – 19 June 2010*
61. Adamson P et al. (MINOS Collab.), arXiv:1006.0996
62. Amsler C et al. (Particle Data Group) *Phys. Lett. B* **667** 1 (2008)
63. de Gouvêa A, Jenkins J, Vasudevan N *Phys. Rev. D* **75** 013003 (2007)
64. Asaka T, Blanchet S, Shaposhnikov M *Phys. Lett. B* **631** 151 (2005)
65. Asaka T, Shaposhnikov M, Kusenko A *Phys. Lett. B* **638** 401 (2006)
66. Fukuda Y et al. (Super-Kamiokande Collab.) *Phys. Rev. Lett.* **85** 3999 (2000)
67. Abe K et al. (Super-Kamiokande Collab.) *Phys. Rev. Lett.* **97** 171801 (2006)
68. Adamson P et al. (MINOS Collab.) *Phys. Rev. Lett.* **101** 221804 (2008); arXiv:0807.2424
69. Sousa A (MINOS Collab.), arXiv:0910.1369

70. Adamson P et al. (MINOS Collab.) *Phys. Rev. D* **81** 052004 (2010); arXiv:1001.0336
71. Autiero D et al. *Nucl. Phys. B Proc. Suppl.* **189** 263 (2009)
72. Gozzi M *Nucl. Phys. B Proc. Suppl.* **172** 152 (2007)
73. Agafonova N et al. *JINST* **4** P06020 (2009); arXiv:0903.2973
74. Acquafredda R et al. (OPERA Collab.) *JINST* **4** P04018 (2009)
75. Lutter G, OPERA Collab., arXiv:0905.4521
76. Marteau J, OPERA Collab., arXiv:0910.3468
77. Agafonova N et al. (OPERA Collab.), arXiv:1006.1623
78. Sato O, talk at *24th Intern. Conf. on Neutrino Physics and Astrophysics*: *NEUTRINO2010, Athens, Greece, 14 – 19 June 2010*
79. Strumia A *Phys. Lett. B* **539** 91 (2002); hep-ph/0201134
80. Aguilar-Arevalo A A et al. (MiniBooNE Collab.) *Nucl. Instrum. Meth. Phys. Res.* **599** 28 (2009); arXiv:0806.4201
81. Roe B P, arXiv:0805.2863, v1
82. Aguilar-Arevalo A A et al. (MiniBooNE Collab.) *Phys. Rev. Lett.* **102** 101802 (2009); arXiv:0812.2243
83. Aguilar-Arevalo A A et al. (MiniBooNe Collab.) *Phys. Rev. Lett.* **103** 111801 (2009); arXiv:0904.1958
84. Aguilar-Arevalo A A et al. (MiniBooNe Collab.), arXiv:1007.1150
85. Maltoni M, Schwetz T *Phys. Rev. D* **76** 093005 (2007); arXiv:0705.0107
86. Sorel M, Conrad J M, Shaevitz M H *Phys. Rev. D* **70** 073004 (2004); hep-ph/0305255
87. Karagiorgi G et al. *Phys. Rev. D* **75** 013011 (2007); hep-ph/0609177
88. Schwetz T, arXiv:0805.2234, v1
89. Murayama H, Yanagida T *Phys. Lett. B* **520** 263 (2001); hep-ph/0010178
90. Gonzalez-Garcia M C, Maltoni M *Phys. Rep.* **460** 1 (2008); arXiv:0704.1800
91. Gershtein S S, Komachenko Yu Ya, Khlopov M Yu *Yad. Fiz.* **33** 1597 (1981) [*Sov. J. Nucl. Phys.* **33** 860 (1981)]
92. Harvey J A, Hill C T, Hill R J *Phys. Rev. Lett.* **99** 261601 (2007); arXiv:0708.1281
93. Alibran P et al. (Gargamelle Collab.) *Phys. Lett. B* **74** 422 (1978)
94. Jenkins J P, Goldman T *Phys. Rev. Lett.* **80** 053005 (2009); arXiv:0906.0984
95. Hill R J, arXiv:1002.4215
96. The MicroBooNE experiment, http://www-microboone.fnal.gov/
97. Maltoni M, Schwetz T, arXiv:0812.3161
98. Schwetz T, Tórtola M, Valle J M F *New J. Phys.* **10** 113011 (2008); arXiv:0808.2016
99. Nakamura K, Particle Data Group *J. Phys. G Nucl. Part. Phys.* **37** 075021 (2010); http://pdg.lbl.gov
100. Lobashev V M et al. *Phys. Lett. B* **460** 227 (1999)
101. Kraus Ch et al. *Eur. Phys. J. C* **40** 447 (2005)
102. Osipowicz A et al., hep-ex/0109033
103. Ichiki K, Takada M, Takahashi T *Phys. Rev. D* **79** 023520 (2009)
104. Reid B A et al. *JCAP* (01) 003 (2010); arXiv:0910.0008
105. Hannestad S *Prog. Part. Nucl. Phys.* **65** 185 (2010)
106. Arafune J, Koike M, Sato J *Phys. Rev. D* **56** 3093 (1997); "Erratum" *Phys. Rev. D* **60** 119905(E) (1999)]
107. Richter B, hep-ph/0008222
108. Sato J, hep-ph/0006127
109. Wolfenstein L *Phys. Rev. D* **17** 2369 (1978)
110. Wolfenstein L *Phys. Rev. D* **20** 2634 (1979)
111. Mikheev S P, Smirnov A Yu *Zh. Eksp. Teor. Fiz.* **91** 7 (1986) [*Sov. Phys. JETP* **64** 4 (1986)]
112. Mikheev S P, Smirnov A Yu *Yad. Fiz.* **42** 1441 (1985) *[Sov. J. Nucl. Phys.* **42** 913 (1985)]
113. Guglielmi A et al., hep-ph/0508034
114. Ardellier F et al. (Double Chooz Collab.), hep-ex/0606025
115. Guo X et al. (Daya Bay Collab.), hep-ex/0701029
116. Barr S M, Dorsner I *Nucl. Phys. B* **585** 79 (2000); hep-ph/0003058
117. Joshipura A S, hep-ph/0411154
118. Nandi S, Tavartkiladze Z *Phys. Lett. B* **661** 109 (2008); arXiv:0708.4033
119. Albright C H *AIP Conf. Proc.* **1222** 98 (2010); arXiv:0911.2437
120. Mezzetto M, Schwetz T *J. Phys. G Nucl. Part. Phys.* **37** 103001 (2010); arXiv:1003.5800
121. Mohapatra R N, Smirnov A Yu *Annu. Rev. Nucl. Part. Sci.* **56** 569 (2006); hep-ph/0603118
122. Kopp S E *Phys. Rep.* **439** 101 (2007); physics/0609129
123. Beavis D et al., "P889, Long Baseline Neutrino Experiment at the AGS", BNL Report No. 52459, April 1995
124. Yamada Y *Nucl. Phys. B Proc. Suppl.* **155** 28 (2006)
125. "T2K ND280 Conceptual Design Report", T2K Internal Document
126. Karlen D *Nucl. Phys. B Proc. Suppl.* **159** 91 (2006)
127. Kudenko Yu *Nucl. Instrum. Meth. Phys. Res. A* **598** 289 (2009)
128. Hamamatsu Photonics K.K., http://www.hamamatsu.com
129. Yokoyama M et al., physics/0605241
130. Gomi S et al. *Nucl. Instrum. Meth. Phys. Res. A* **581** 427 (2007)
131. Yokoyama M et al. *Nucl. Instrum. Meth. Phys. Res. A* **610** 128 (2009); arXiv:0807.3145
132. Mineev O et al. *Nucl. Instrum. Meth. Phys. Res. A* **577** 540 (2007)
133. Izmaylov A et al. *Nucl. Instrum. Meth. Phys. Res. A* **623** 382 (2010); arXiv:0904.4545
134. Hayato Y, T2K Collab. *Nucl. Phys. B Proc. Suppl.* **143** 269 (2005)
135. Hayato Y *Nucl. Phys. B Proc. Suppl.* **112** 171 (2002)
136. The T2K experiment, http://www.t2k.org
137. Marciano W J, hep-ph/0108181
138. Bernabeu J, Espinoza C, arXiv:0905.2913
139. Rubbia A *J. Phys. Conf. Ser.* **171** 012020 (2009); arXiv:0908.1286
140. Badertscher A et al., arXiv:0804.2111
141. Barger V et al., arXiv:0705.4396
142. Hasegawa T, arXiv:1001.0452
143. Zucchelli P *Phys. Lett. B* **532** 166 (2002)
144. Geer S *Phys. Rev. D* **57** 6989 (1998); "Erratum" *Phys. Rev. D* **59** 039903(E) (1999); hep-ph/9712290
145. Volpe C *J. Phys. G Nucl. Part. Phys.* **34** R1 (2007); hep-ph/0605033
146. Autin B et al. *J. Phys. G Nucl. Part. Phys.* **29** 1637 (2003)
147. Terranova F et al. *Eur. Phys. J. C* **38** 69 (2004)
148. Agarwalla S K, Huber P, arXiv:0909.2257
149. Budker G I, in *Proc. 7th Int. Conf. on High Energy Accelerators, Yerevan, 1969*, p.33
150. Skrinskii A N, Parkhomchuk V V *Fiz. Elem. Chastits i At. Yadra* **12** 557 (1981) [*Sov. J. Part. Nucl.* **12** 223 (1981)]
151. Bandyopadhyay A et al. *Rep. Prog. Phys.* **72** 106201 (2009)
152. Abe T et al. *JINST* **4** T05001 (2009)
153. Mezzetto M, arXiv:0905.2842